Magnetic fabric in carbonatic rocks from thrust shear zones: A study from the Northern Apennines (Italy)

DOI:10.1016/j.tecto.2020.228573

Magnetic Fabric in Thrust Shear Zones: A Study from the Northern Apennines (Italy)

Sara Satolli [a,b,*], Claudio Robustelli Test [b,c], Dorota Staneczek [d], Elena Zanella [b,c], Fernando Calamita [a], Evdokia Tema [b,c]

[a] Dipartimento di Ingegneria e Geologia, Università degli Studi "G. d'Annunzio" di Chieti-Pescara, via dei Vestini 31, 66100 Chieti, Italy

[b] CIMaN-ALP, Centro Interuniversitario di Magnetismo Naturale - Alpine Laboratory of Paleomagnetism, via Luigi Massa 4, 12016 Peveragno, Italy

[c] Dipartimento di Scienze della Terra, Università degli Studi di Torino, via Valperga Caluso 35, 10125 Torino, Italy

[d] Institute of Geophysics, Polish Academy of Sciences, Księcia Janusza 64, 01-452, Warszawa, Poland

[*] Corresponding author at: Dipartimento di Ingegneria e Geologia, Università degli Studi "G. d'Annunzio" di Chieti-Pescara, via dei Vestini 31, 66100 Chieti, Italy, Tel.: 0039 0871 355 6427, e-mail address: sara.satolli@unich.it

ABSTRACT

We present the results of an integrated structural and anisotropy of magnetic susceptibility (AMS) investigation in thrust shear zones. A total of 17 sites from six localities along the frontal and oblique ramp of the Olevano-Antrodoco-Sibillini thrust and back thrust (Northern Apennines, Italy) were studied to investigate both magnetic fabric and structural characteristics of Cretaceous to Neogene calcareous and marly rocks. In most of the sites AMS is controlled by the paramagnetic minerals (prevailingly phyllosilicates). Structural analysis shows the presence of SC- and S-tectonites associated to predominant simple and pure shear, respectively. The combination of density diagrams and cluster analysis allowed discriminating different sedimentary/tectonic overprints on a blended magnetic fabric. Six different subfabrics were distinguished, related to the structural data and associated to deformation stages and regimes. The magnetic foliation has a double tendency to parallelize to pressure solution cleavage (S) and shear planes (C). The magnetic lineation tends to progressively align with the slip vector, save for pure-shear-dominated sites at less than 15-20 cm from the thrust, where it aligns with the transport direction. The magnetic fabric is dominated by simple shear deformation. The protocol applied for AMS analysis shows a great potential to unravel blended sedimentary and/or tectonic features in magnetic fabrics. AMS can be considered as a useful tool in unravelling the variation of simple-pure shear deformation regime in shear zones.

Keywords: Magnetic fabric; Structural geology; Pure shear; Simple shear; Tectonites

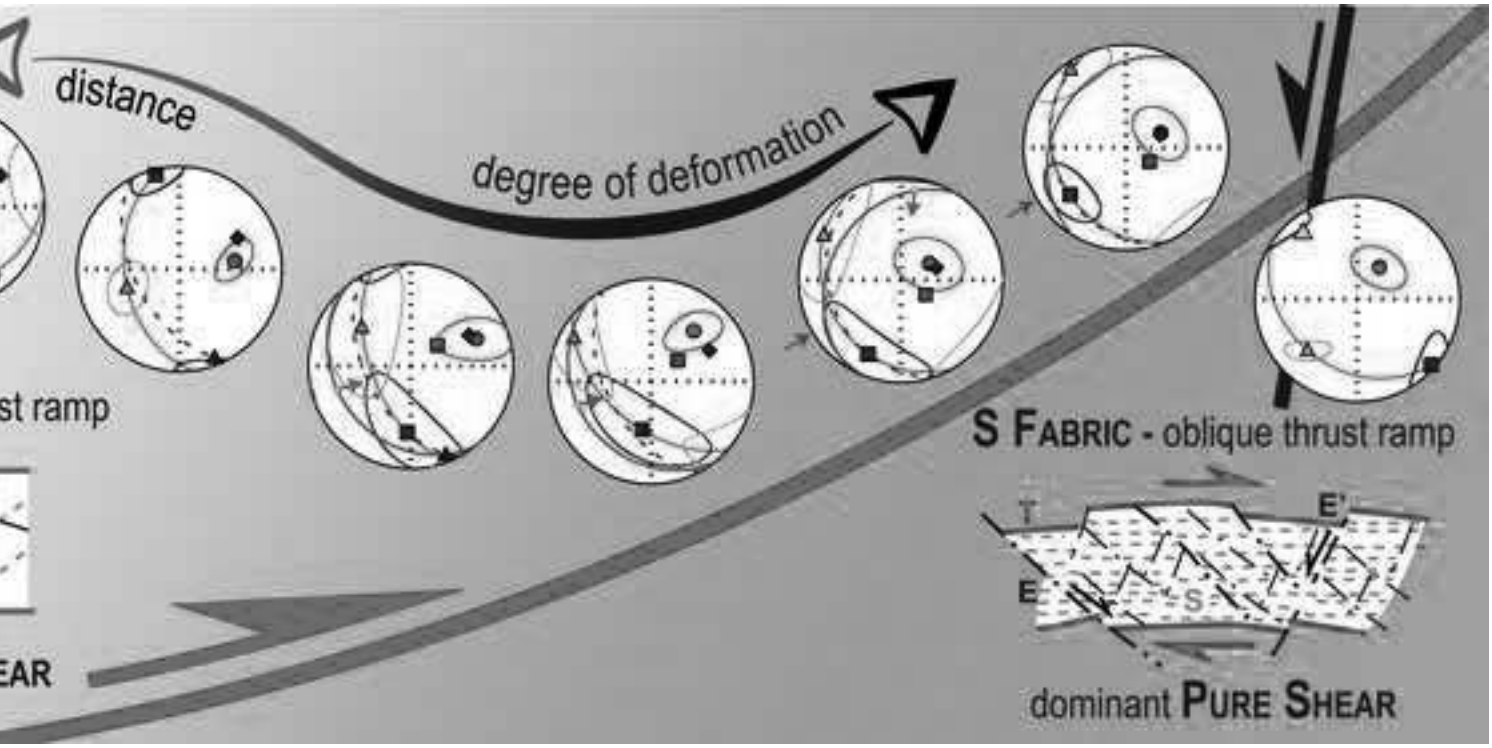

distance
degree of deformation
st ramp
EAR
S FABRIC - oblique thrust ramp
T
E'
E
S
dominant PURE SHEAR

Highlights

- we performed a magnetic fabric investigation on simple-to-pure-regime shear zones
- density diagrams and cluster analysis allowed distinguishing different processes
- six different fabrics were recognized depending on the intensity of deformation
- the magnetic fabric is more sensitive to the simple shear deformation

Magnetic Fabric in Thrust Shear Zones: A Study from the Northern Apennines (Italy)

Sara Satolli [a,b,*], Claudio Robustelli Test [b,c], Dorota Staneczek [d], Elena Zanella [b,c], Fernando Calamita [a], Evdokia Tema [b,c]

[a] Dipartimento di Ingegneria e Geologia, Università degli Studi “G. d’Annunzio” di Chieti-Pescara, via dei Vestini 31, 66100 Chieti, Italy

[b] CIMaN-ALP, Centro Interuniversitario di Magnetismo Naturale - Alpine Laboratory of Paleomagnetism, via Luigi Massa 4, 12016 Peveragno, Italy

[c] Dipartimento di Scienze della Terra, Università degli Studi di Torino, via Valperga Caluso 35, 10125 Torino, Italy

[d] Institute of Geophysics, Polish Academy of Sciences, Księcia Janusza 64, 01-452, Warszawa, Poland

[*] Corresponding author at: Dipartimento di Ingegneria e Geologia, Università degli Studi “G. d’Annunzio” di Chieti-Pescara, via dei Vestini 31, 66100 Chieti, Italy, Tel.: 0039 0871 355 6427, e-mail address: sara.satolli@unich.it

ABSTRACT

We present the results of an integrated structural and anisotropy of magnetic susceptibility (AMS) investigation in thrust shear zones. A total of 17 sites from six localities along the frontal and oblique ramp of the Olevano-Antrodoco-Sibillini thrust and back thrust (Northern Apennines, Italy) were studied to investigate both magnetic fabric and structural characteristics of Cretaceous to Neogene calcareous and marly rocks. In most of the sites AMS is controlled by the paramagnetic minerals (prevailingly phyllosilicates). Structural analysis shows the presence of SC- and S-tectonites associated to predominant simple and pure shear, respectively. The combination of density diagrams and cluster analysis allowed discriminating different sedimentary/tectonic overprints on a blended magnetic fabric. Six different subfabrics were distinguished, related to the structural data and associated to deformation stages and regimes. The magnetic foliation has a double tendency to parallelize to pressure solution cleavage (S) and shear planes (C). The magnetic lineation tends to progressively align with the slip vector, save for pure-shear-dominated sites at less than 15-20 cm from the thrust, where it aligns with the transport direction. The magnetic fabric is dominated by simple shear deformation. The protocol applied for AMS analysis shows a great potential to unravel blended sedimentary and/or tectonic features in magnetic fabrics. AMS can be considered as a useful tool in unravelling the variation of simple-pure shear deformation regime in shear zones.

Keywords: Magnetic fabric; Structural geology; Pure shear; Simple shear; Tectonites

1. Introduction

Shear zones are zones of localized high deformation that can develop in any tectonic regime, involving simple shear or a combination of simple and pure shear (Ramsay and Graham, 1970; Ramsay, 1980; Ramsay and Huber, 1987). Tectonites in simple shear regime are characterized by the association of two planar structures (Ramsay and Graham, 1970; Berthé et al., 1979; Lister and Snoke, 1984): C shear planes due to localized shear strain, being parallel to the main fault, and S pressure-solution cleavage due to the accumulation of finite strain (Jégouzo, 1980; Ponce de Leon and Choukroune, 1980). Surfaces S and C initially form with a 45° angle (SC tectonites) that can gradually decrease to 0° with progressive shear. At the last stage of deformation, the S and C planes become sub-parallel (S tectonite). For example, S-fabric characterizes oblique thrust ramps related to the transpressive reactivation of the pre-existing normal faults (Pace et al., 2015).

Other structures associated to tectonites are calcite tension veins orthogonal to S that are shortened and stretched as the deformation and density of surfaces increase (Ramsay, 1980); calcite shear veins on C, synthetic (R) and subordinated antithetic (R') shear planes, respectively at ca. 15° and 75° with respect to C (Riedel, 1929). This geometry may be more complex in sub-simple shear zones due to the presence of composed fabrics, as in the case of flanking structures or folded fabrics (e.g., Passchier, 2001, Calamita et al., 2012, Pace et al., 2015). Both synthetic and antithetic extensional shear surfaces can be observed associated with the thrust or displacing it at different stages of the deformation (e.g., Platt and Vissers, 1980; Platt, 1984; Harris and Cobbold, 1985; Holdsworth et al., 2006). Moreover, conjugate extensional shear planes develop along oblique thrust ramps associated with a significant component of pure shear (Calamita et al., 2012; Pace et al., 2015).

Shear zones can occur at very different scales, but many of their aspects are scale independent, always showing the same characteristics (Fossen and Cavalcante, 2017). However, in an ideal shear zone the strain is maximum in its central part and a progressive rotation occurs from the margin to the central part (Fossen, 2010).

The aim of this study is to investigate how structural deformation differences in shear zones are documented by the anisotropy of magnetic susceptibility (AMS). In fact, AMS can detect the preferred orientation of para- and ferromagnetic minerals in rocks, even when the micro- or macroscopic strain markers are missing. The principal magnetic susceptibility axes are related to the tectonic stress and structural features, offering important information on the sedimentary and/or tectonic setting of a studied area. The magnetic fabric of deformed rocks has been widely investigated to quantify the progressive ductile deformation, both experimentally and theoretically (e.g., Graham, 1966; Hrouda and Jezék, 1999; Borradaile and Henry, 1997; Borradaile and Hamilton, 2004; Weil and Yonkee, 2009; Parés, 2015; Almqvist and Koyi, 2018; Hrouda and Chadima, 2019). In undeformed sedimentary rocks, AMS is defined by a magnetic foliation parallel to the bedding. The minimum susceptibility axes (k_3) are vertical, while the maximum susceptibility (k_1) axes are scattered in the horizontal plane. With layer-parallel shortening, a tectonic foliation develops and evolves with the increasing of deformation: first, the k_1 axes become subhorizontal and perpendicular to the shortening direction, then k_3 axes form a girdle parallel to the shortening direction, and finally k_3 axes group subhorizontally and parallel to the shortening direction (Weil and Yonkee, 2009 and references therein). The deformation of magnetic minerals in a ductile shear zone may be ascribed to different deforming mechanisms such as grain rotation, recrystallization and plastic deformation (Sidman et al., 2005; Ferré et al., 2014). Furthermore, the deformation mechanisms primarily depend on differential stress, tectonic regimes and on the mineralogical source of the AMS (e.g., Borradaile and Alford, 1988; Housen et al., 1995; Parés and van der Pluijm, 2002).

We present here the results of a detailed AMS fabric investigation applied on shear zones from 3 sectors of the Northern Apennines fold-and-thrust belt. These sectors are characterized by different combinations of simple and pure shear, which has been quantified through the vorticity number W_k (Xypolias, 2010; Calamita et al., 2012; Pace et al., 2015).

2. Geological Setting

The Triassic to Miocene sedimentary successions of the Northern Apennines were deposited on the Adria paleomargin (Ciarapica and Passeri, 2002) and involved in the orogenesis during the Neogene–Quaternary due to the convergence between Africa and Europe (e.g., Boccaletti et al., 2005).

The study area is located in Pliocene outer thrust of the Northern Apennines, known as the Olevano-Antrodoco-Sibillini (OAS) thrust (Fig. 1). The outer thrust shows a curved shape defined by frontal NW-SE-trending and oblique NNE-SSW-trending thrust ramps to the north and to the south of its apical zone, respectively. To the north, the OAS juxtaposes the Jurassic–Cretaceous carbonate platform and pelagic sequence on the Oligocene-Miocene hemipelagic marly succession (Scaglia Cinerea, Marne con Cerrogna and Laga Fms.) belonging to the Umbria-Marche domain. To the south the footwall is represented, instead, by a persistent carbonate platform domain (Lazio-Abruzzi domain).

The Jurassic-Eocene sequence was deposited on the Adria paleomargin during the opening of the Tethys ocean. Starting from the middle–late Miocene, the deformation switched from extension to compression in a context of positive inversion tectonics, where pre-thrusting normal faults were reactivated with different geometries (e.g., Tavarnelli et al., 2004; Butler et al., 2006; Calamita et al., 2012). The southern NNE-SSW trending sector of the OAS

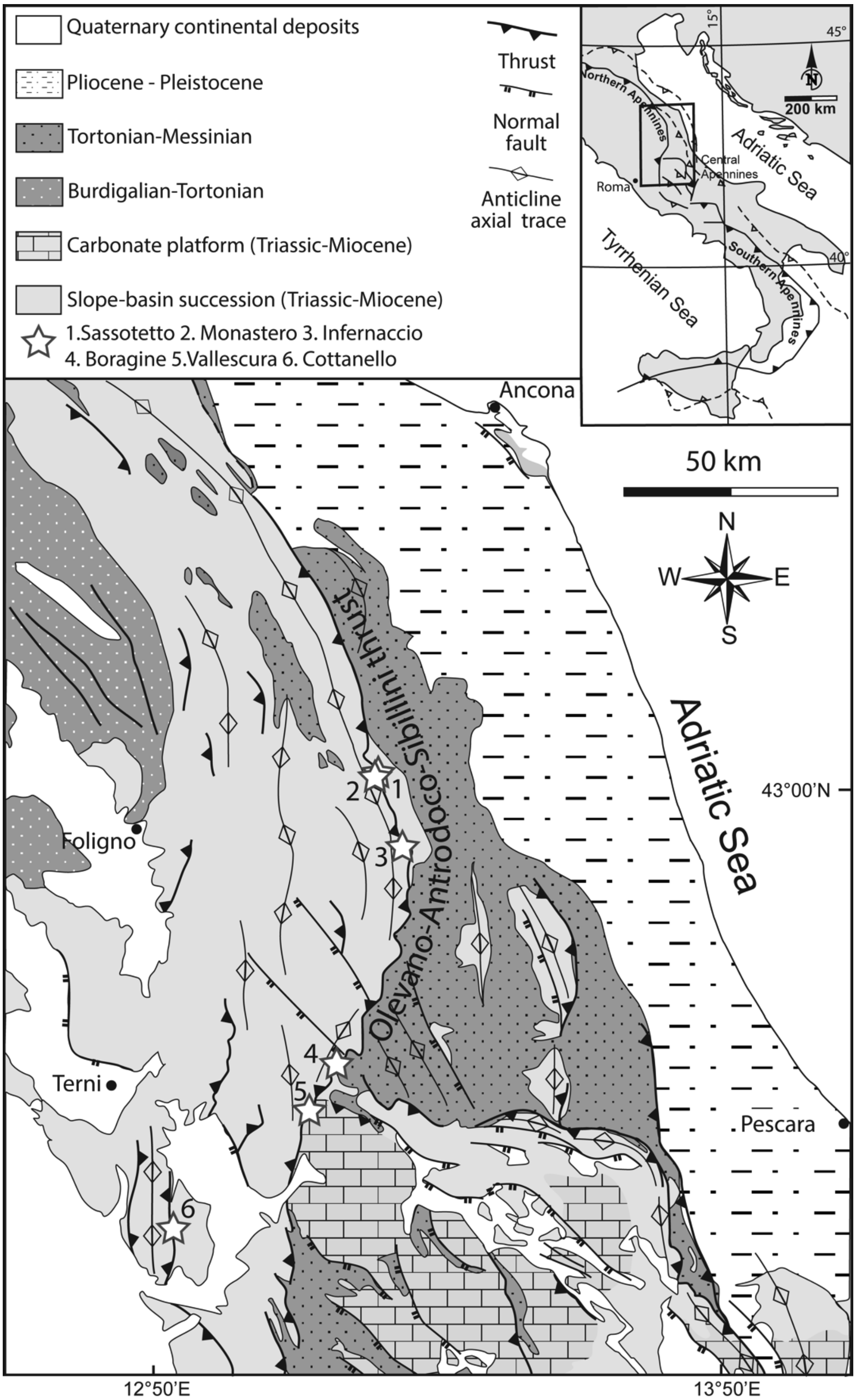

Figure 1: Schematic geological map of the Northern Apennines (Italy) with the studied localities (white stars), modified after Calamita et al. (2012). The curve-shaped Olevano-Antrodoco-Sibillini (OAS) thrust is the outer front of the Northern Apennines.

reactivated the Lower Jurassic normal fault that separated the carbonate platform from the pelagic domains (Ancona-Anzio fault, Castellarin et al., 1982); after its emplacement, it was antiformally folded by anticlines developed in its footwall (Alberti et al., 1996).

During the Quaternary, post-orogenic extension, characterized by hinterland-dipping NW–SE-trending normal faults with associated intermontane basins and seismicity, affected the axial zone of Northern Apennines belt (Calamita et al., 2000; Di Domenica et al., 2012).

In the Northern Apennines, tectonites have been largely documented (Koopman, 1983; Lavecchia, 1985; Calamita et al., 1987; Ghisetti, 1987; Calamita, 1991; Calamita et al., 1991, 2012; Alberti et al., 1996; Pierantoni, 1996; Tavarnelli, 1997, 1999). They are usually associated with the outer thrust, showing different characteristics along two differently oriented thrust ramps (Calamita et al., 2012).The NNE-SSW-trending oblique thrust ramp is characterized by the presence of S tectonites, while the NW-SE-trending frontal ramp is characterized by the presence of SC tectonites. The combination of simple and pure shear, thus the degree of non-coaxiality of these shear zones has been quantified through the kinematic vorticity number, allowing to discriminate simple-shear- and pure-shear-dominate deformation (Xypolias, 2010; Calamita et al., 2012).

The lithologies most commonly affected by tectonites are Scaglia Rossa, Scaglia Cinerea and Marne con Cerrogna. The Scaglia Rossa Fm. (Lower Turonian-middle Eocene) predominantly consists in pink and red limestones and marly limestones with chert bands and nodules, and average 20 cm bed thickness. It can be divided in 4 members: i. red/pinkish limestones with dark/red chert; ii. pinkish/reddish limestones without chert; iii. marly limestones without chert; iv. red marly limestones with cherts. The Cretaceous/Paleogene boundary is between facies (ii) and (iii) that are also grouped in the same member in some geological maps. The non-carbonatic component is represented by quartz, mica-illite, montmorillonite, hematite, magnetite and occasionally pyrite (Arthur and Fisher, 1977; ISPRA, 2007). After the Scaglia Rossa Fm., there is a transition from pelagic to turbidite sedimentation with an increase of the marly component. The Scaglia Cinerea Fm. (Upper Eocene- Lower Miocene) is represented by greyish/greenish marly limestones and marls with thin bedding. It can be divided in 3 facies: i. grey/reddish limestones; ii. greyish/greenish marls; iii. greyish marls and clay. The Marne con Cerrogna (Burdigalian-middle Tortonian) consists of medium to thickly bedded alternating marls, calcareous marls and clay marls, intercalated with calcareous turbidites (Centamore and Micarelli, 1991).

3. Methods

We sampled tectonites from different sectors of the Northern Apennines (Fig. 1) in order to characterize their magnetic fabric at several localities on the frontal (Sassotetto, Monastero, Infernaccio) and oblique (Boragine, Vallescura) ramps of OAS, and on a back thrust from the inner sector of the Northern Apennines (Cottanello) .

3.1 Structural analysis

Structural data were collected to analyze the local trends of the main structures and the slip vector was calculated on the stereonet after measuring S and C surfaces.

Three localities, Sassotetto (43°01’09.0”N, 13°14’54.2”E), Monastero (43°03’30.6”N, 13°13’53.0”E) and Infernaccio (42°55’24.5”N, 13°16’50.0”E), were selected in the frontal NW-SE-trending OAS thrust. This sector is characterized by a well-developed brittle–ductile shear zone, with SC tectonites of decametric thickness, mostly involving the micritic pelagic limestones of the Scaglia Rossa Fm. and the marly lithologies of the Scaglia Cinerea Fm. in a simple shear dominated deformation regime characterized by a vorticity number close to 1 (W_k

= 0.96 - 0.99; Calamita et al., 2012).

Two localities, Boragine (42°29’30.7”N, 13°03’05.5”E) and Vallescura (42°34’47,6”N, 13°08’21,1”E) are located in the NNE-SSW-trending OAS thrust, that emplaces the pelagic carbonates of Scaglia Rossa Fm. onto the marls and shales of the Marne con Cerrogna Fm.. Here, the shear zone is characterized by S tectonites developed in a pure shear-dominated regime with a W_k varying between 0.27 and 0.76 (Calamita et al., 2012; Pace et al., 2015).

Finally, one locality, Cottanello (42°25’00,9”N, 12°41’25,1”E) was selected in the inner sector of the Apennines, ca. 40 km west of the NNE–SSW-trending OAS oblique thrust ramp, in proximity of a N10 trending structure known in the literature as the Sabina Fault. This feature shows complex kinematics with slip vectors in three different directions: NE-SW, NNE-SSW and E-W (Pierantoni, 1996). In the literature, it was interpreted as a dextral strike-slip (Alfonsi et al., 1995) or transpressive fault characterized by kinematics partitioning (Pierantoni, 1996), or as an east-dipping high-angle back-thrust reactivating pre-existing normal faults bounding a symmetric Jurassic basin (Scisciani, 2009; Calamita et al., 2011; Di Domenica et al., 2012; Pace and Calamita, 2014).

3.2 Anisotropy of magnetic susceptibility

3.2.1 Sampling

From each locality, 1 to 5 sites were sampled and studied. Both site size and sampling strategy were decided based on the homogeneity and pervasivity of the tectonic structures as well as on the outcrop conditions. However, in order to obtain significant statistical analysis, at least 10 oriented hand samples of 10-20 cm lithons were collected at each site. Sites were named accordingly to the locality (first letter: S = Sassotetto; I = Infernaccio; M = Monastero; B = Boragine; V = Vallescura; C = Cottanello), the lithology (second and third letters: SR = Scaglia

Rossa Fm.; SC = Scaglia Cinerea Fm.; MC = Marne con Cerrogna Fm.) and the distance from the fault plane (progressive numbers with the distance increment) or sublocality.

Along the frontal thrust ramp, the hanging wall was sampled at Sassotetto at ca. 15-20 m from the main thrust, while the footwall was sampled at Monastero at ca. 15 m (MSC1) and ca. 45 m (MSC2), and at Infernaccio at ca. 30 m below the main thrust.

From the oblique thrust ramp at Boragine and Vallescura, we sampled different levels at a progressively increasing distance of 15-20 cm from the main thrust. In both localities, 2 sites in the hanging wall into the Scaglia Rossa Fm. and 3 sites in the footwall into the Marne con Cerrogna Fm. were sampled.

Finally, at Cottanello we sampled 3 different 1-m-wide levels located at progressively increasing distance from the main fault.

All collected blocks were oriented *in situ* with a compass and an inclinometer. From each block several specimens were prepared at the laboratory, weighed and centered into plastic boxes (2 cm x 2 cm x 2 cm) where they were fixed with non magnetic plasticine. A total of 327 oriented specimens was obtained from 17 sites.

3.2.2 Laboratory Analysis and data processing

For each specimen, the AMS was measured with an AGICO KLY-3 Kappabridge (sensitivity of 2×10^{-8} SI), at the CIMaN-ALP (Centro Interuniversitario di Magnetismo Naturale - Alpine Laboratory of Paleomagnetism, Peveragno, Italy). Measurements were conducted using the manual mode (15 different directions) at the instrument's operating frequency of 875 Hz and field intensity of 300 Am^{-1}. In order to maximize the holder correction, critical in the case of samples with very low susceptibility values, we executed it on the holder, plastic box and plasticine ensemble. Then, the mass magnetic susceptibility (χ_m) was computed for each specimen.

All measurements were subjected to a quality check. Only measurements with all three F-statistics of the anisotropy tests (F, F_{12} and F_{23}) higher than 5 were accepted as reliable. $F > 3.4817$ indicates a statistically anisotropic specimen within the 95% of likelihood, and F_{12}, $F_{23} > 4.2565$ allow to reject the null-hypothesis of rotational symmetry (Hrouda, 2002 and references therein). In addition, few outliers characterized by $\pm 2\sigma$ difference with respect to the mean of AMS scalar parameters were excluded from further analysis.

On the retained specimens, the magnetic fabric was reconstructed at site level by computing the AMS second rank tensor using the software ANISOFT (Chadima and Jelínek, 2008), based on Jelínek statistics (Jelínek, 1977). The anisotropy tensor is represented as a tri-axial ellipsoid ($k_1 \geq k_2 \geq k_3$), whose axes orientation and magnitude depends on the relative abundance of mineral species and their grain orientations. Particularly, the k_3 axis represents the pole of the magnetic foliation plane and the k_1 direction defines the magnetic lineation. The AMS ellipsoid shape is defined by the scalar parameter T and can vary from oblate ($0 \leq T \leq +1$) to prolate ($-1 \leq T \leq 0$) (Jelínek, 1981). The intensity of the preferred orientation of magnetic minerals, which results in the eccentricity of the AMS ellipsoid, is represented by the parameter P' (Jelínek, 1981), called the corrected degree of anisotropy. A progressive tectonic deformation and a partial fabric overprinting due to different mineralogy behavior may result in a blended magnetic fabric (Borradaile and Jackson, 2004).

In order to define the presence of different subfabrics at site level, we first removed outliers characterized by significant variations of χ_m, P' and/or T parameters, and we then identified clusters of AMS scalar parameters. When clusters were not defined by these parameters and blended fabrics were clearly displayed, we applied a combination of contouring and cluster analysis on each principal axis to identify different subfabrics (Borradaile and Jackson, 2004;

Borradaile and Jackson, 2010; Aubourg et al., 2010; Caricchi et al., 2016; Robustelli Test et al., 2019). Subfabrics were detected computing the cluster analysis with the Stereo32 software (Röller and Trepmann, 2008) and were validated using P', T and χ_m variations. In this way, we distinguished groups of specimens affected by different sedimentary or tectonic processes.

4. Results

4.1 Structural data

4.1.1 Shear zones along frontal thrust ramps

The SC tectonites show centimeter-to-decameter spaced C shear planes with calcite-bearing shear veins sub-parallel to the main thrust and centimeter-spaced S pressure solution cleavage, identifying spaced and elongated sigmoidal-shaped calcareous lithons. Millimeter- to centimeter-scale tension veins filled with calcite are perpendicular to the S foliation and low-angle synthetic R planes are also present.

Sassotetto and Monastero are located at the hanging wall and footwall of the same thrust shear zone, respectively. Sassotetto was sampled in the Scaglia Rossa Fm. and shows C planes oriented at 250/24 and S fabric oriented at 231/57. Monastero is located in the footwall of the same thrust zone in the Scaglia Cinerea Fm. and shows C planes oriented at 232/27 and S planes oriented at 242/54. Infernaccio is also located in the footwall of the thrust shear zone juxtaposing the Scaglia Rossa on the Scaglia Cinerea Fm. Here, the kinematic analysis shows C planes oriented at 230/20 and S planes oriented at 254/61 (Calamita et al., 2012) while synthetic R planes are oriented at 248/09.

In this sector, the SC intersection is NW-SE with a slip vector indicating a NE displacement direction (Fig. 2).

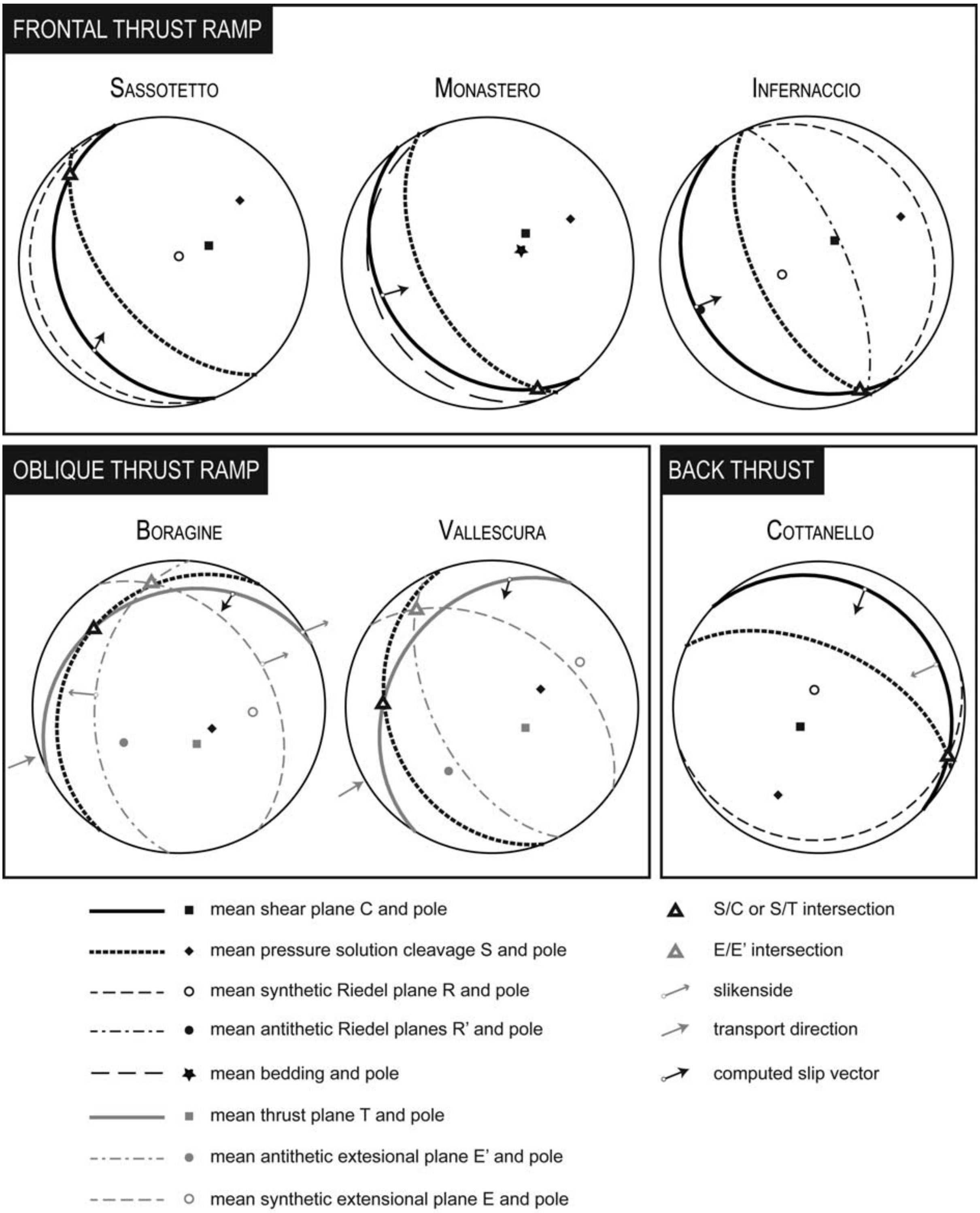

Figure 2: Summary of the structural data for each studied locality integrated with data from the literature (Calamita et al., 2012; Turtù et al., 2013; Pace et al., 2015).

4.1.2 Shear zones along oblique thrust ramps

The S surfaces are sub-parallels to the main thrust plane, identifying marly–calcareous lens-shaped lithons. The foliation is more pervasive in the marls and shales lithotypes of the Marne con Cerrogna, and is decimeter-spaced in the marly/calcareous Scaglia Rossa Fm.. Furthermore, synthetic and antithetic extensional structures displace the main thrust surface and the associated shear zone.

At Boragine the thrust plane (T) is oriented 334/29 and the S surfaces are oriented 303/22, with a NW-SE-trending S/T intersection. Synthetic and antithetic plane E and E' are oriented 057/37 and 274/42, respectively (Calamita et al., 2012; Turtù et al., 2013). At Vallescura the thrust plane is oriented 302/30 and the S surfaces are oriented 250/29. Synthetic and antithetic planes E and E' are oriented 394/44 and 243/57, respectively (Calamita et al., 2012).

In both localities, the N60-70 transport direction (Calamita et al., 2012) differs from the S-SSW computed slip vector (Fig. 2).

4.1.3 Back-thrust in a transpressive context

Cottanello is characterized by sub-simple shear with $W_k = 0.72$ (Pace et al., 2015). Here, SC tectonites are well developed in the Scaglia Rossa Fm. and exposed in a quarry of the Roman period (San Pietro quarry). The tectonites are characterized by centimeter-spaced C planes oriented 244/75 and millimeter- to centimeter-spaced S surfaces oriented 025/52. Frequent low-angle R synthetic planes cross the shear zone at ca. 20° to the C-surfaces (Pace et al., 2015). The slip vector is toward S-SSW, while slickensides indicate a NE-E direction (Fig. 2).

4.2 AMS results

All the sampled lithologies show consistent P’ and T parameters (Table 1; Fig. 3B-C). Their magnetic ellipsoids are mainly neutral to slightly oblate with mean T = 0.136 ± 0.307. Overall, P’ is moderate with mean values of P’ = 1.058 ± 0.053. Mass-susceptibility is generally low (mean value χ_m = 11.8 ± 12.27 [x 10^{-9} m^3kg^{-1}]) but varies depending on the lithology (Fig. 3A): χ_m = 28.80 ± 15.11 [x 10^{-9} m^3kg^{-1}] in the Scaglia Cinerea Fm.; χ_m = 8.22 ± 5.61 [x 10^{-9} m^3kg^{-1}] in the Marne con Cerrogna Fm., and χ_m = 5.77 ± 5.16 [x 10^{-9} m^3kg^{-1}] in the Scaglia Rossa Fm.. The complete list of specimens and their parameters is reported in Supplementary Table 1 and 2 for the specimens and at site level, respectively.

Those values indicate that the magnetic fabric is dominated by the contribution of paramagnetic minerals such as clay minerals (Tarling and Hrouda,1993), save for two sites from the Scaglia Rossa Fm. located at Boragine. In these cases, diamagnetic minerals are the main carrier of the magnetic fabric, probably also due to the high pervasivity of calcite veins. Significative low values of magnetic susceptibility in the Scaglia Rossa Fm. were also reported in previous studies (Mattei et al., 1995). The occurrence of diamagnetic phases might reveal the presence of inverse fabric in those sites.

4.2.1 AMS from the frontal thrust ramps

All sites show a well-defined magnetic fabric with clustered k_3 and slightly dispersed k_1 and k_2 axes. The magnetic foliation is mostly WSW-dipping at medium to high angle, save for site MSC2 (see Fig. 5), which shows a S-dipping sub-horizontal magnetic foliation. The shape of the ellipsoid is mainly oblate with T values up to 0.902. The degree of anisotropy P’ is moderate, ranging from 1.015 to 1.147. Variations of P’ occur in relation to the different sampled lithologies and distances from the main thrust (Fig. 3B and Fig. 4A-C).

Locality	Site	Stage	n/N	χ_m (± σ)	P'	T	k_1				k_3			
				(x 10^{-9} m^3kg^{-1})			D	I	95% conf. angles		D	I	95% conf. angles	
Sassotetto	SSR1		16/20	11.16 ± 5.19	1,040	0,785	295	32	52,1	18,3	47	31	21,1	11,6
	SSR1-SF1	E	10/16	12.71 ± 5.76	1,030	0,671	191	50	56,7	22,9	40	36	26,8	12,9
	SSR1-SF2	C	6/16	8.56 ± 2.86	1,061	0,386	304	29	18,6	8,8	51	28	13,3	8,6
Monastero	MSC1		19/20	39.65 ± 21.54	1,021	0,613	342	5	35,1	13,5	76	39	18,6	12,1
	MSC1-SF1	C	8/19	17.20 ± 4.45	1,021	0,903	161	2,3	77,5	12,0	70	32	14,4	8,9
	MSC1-SF2	C	11/19	55.98 ± 11.19	1,023	0,465	346	6	19,2	13,2	82	45	20,2	10,7
	MSC2		19/19	24.69 ± 2.66	1,017	0,648	133	13	59,4	13,0	1	71	22,2	13,8
	MSC2-SF1	A	10/19	24.12 ± 1.91	1,019	0,158	100	1	31,8	12,9	8	77	17,0	11,4
	MSC2-SF2	B	9/19	25.32 ± 3.39	1,020	0,052	169	22	28,5	14,2	351	68	32,5	14,2
Infernaccio	ISC1		19/21	22.07 ± 7.02	1,032	0,856	212	50	75,1	24,4	76	32	30,1	24,6
	ISC1-SF1	D	14/19	18.63 ± 2.86	1,014	0,479	183	35	53,3	21,6	68	31	33,8	14,9
	ISC1-SF2	E	5/19	31.71 ± 6.10	1,117	0,657	297	59	17,9	7,7	79	25	18,7	7,6
Monte Boragine	BSR2	F*	10/15	-2.03 ± 0.98	1,076	-0,351	319	59	68,7	18,1	180	25	31,9	16,0
	BSR1	F*	10/19	-3.33 ± 1.81	1,027	-0,656	169	80	70,0	31,0	9	10	43,3	23,9
	BMC1	E$^{//}$	8/12	2.52 ± 1.94	1,055	0,147	250	46	59,9	27,9	4	21	52,9	20,8
	BMC2		13/16	9.83 ± 6.33	1,032	0,593	243	13	43,6	17,3	128	61	25,7	17,3
	BMC2-SF1	E or E$^{//}$	6/13	6.44 ± 2.28	1,027	0,175	35	6	37,0	23,4	134	57	31,3	14,7
	BMC2-SF2	D$^{//}$	7/13	12.74 ± 7.37	1,040	0,410	266	23	30,8	18,2	121	63	22,4	14,2
	BMC3		15/21	1.05 ± 2.96	1,121	-0,037	201	21	44,2	24,5	9	69	59,4	23,6
	BMC3-SF1	E or E$^{//}$	8/15	3.34 ± 1.96	1,035	-0,225	211	1	49,7	20,5	304	72	45,3	28,5
	BMC3-SF2	D*	7/15	-1.56 ± 1.00	1,080	0,071	197	29	34,2	19,9	29	61	54,6	15,2
Valle Scura	VSR2		19/21	7.23 ± 1.88	1,022	0,010	207	25	32,2	17,8	31	65	35,3	16,6
	VSR2-SF1	E$^{//}$	14/19	7.12 ± 1.80	1,027	-0,383	211	25	23,3	16,7	28	65	43,5	15,2
	VSR2-SF2	F	5/19	7.52 ± 2.29	1,020	-0,134	132	4	23,0	12,1	35	59	22,7	15,6
	VSR1	E$^{//}$	23/24	9.29 ± 2.17	1,039	0,091	230	28	24,3	18,0	67	61	24,3	18,0
	VMC1		18/21	8.56 ± 3.56	1,015	0,529	263	21	68,5	14,8	29	57	33,5	18,7
	VMC1-SF1	E$^{//}$	10/18	8.16 ± 2.22	1,020	-0,346	227	26	22,5	18,6	1	55	45,1	21,6
	VMC1-SF2	F	8/18	9.07 ± 4.89	1,023	-0,361	303	5	28,3	9,6	38	42	46,0	10,3
	VCM2		19/21	12.25 ± 2.37	1,024	0,406	234	21	49,0	15,8	37	68	22,7	15,8
	VMC2-SF1	D$^{//}$	9/19	12.25 ± 2.37	1,032	-0,004	253	19	11,6	10,5	43	68	28,2	8,7
	VMC2-SF2	E	10/19	12.42 ± 1.51	1,020	0,186	191	20	25,6	14,1	28	69	26,8	14,9
	VCM3		18/21	11.56 ± 3.62	1,022	0,442	204	22	44,0	20,6	60	64	28,3	20,1
	VMC3-SF1	D$^{//}$	8/18	11.44 ± 3.24	1,025	0,120	244	38	30,4	17,3	64	53	23,6	21,8
	VMC3-SF2	E	10/18	12.18 ± 4.37	1,025	0,181	185	12	21,0	15,1	37	77	25,9	16,3
Cottanello	CSR1		13/15	2.97 ± 1.21	1,025	-0,056	317	35	50,4	26,9	204	29	39,4	26,3
	CSR1-SF1	D	6/13	2.4 ± 1.37	1,039	0,113	325	42	53,5	22,8	188	39	36,8	21,3
	CSR1-SF2	C	7/13	3.47 ± 0.86	1,019	0,097	312	17	51,2	11,4	221	5	30,5	11,4
	CSR2		16/22	5.72 ± 2.79	1,026	0,058	329	22	47,5	25,1	167	67	47,6	23,0
	CSR2-SF1	E	8/16	5.91 ± 2.78	1,045	0,222	13	40	22,2	13,5	188	50	14,6	13,0
	CSR2-SF2	C	8/16	5.52 ± 2.97	1,038	0,329	324	4	32,8	12,9	60	57	27,4	13,6
	CSR3		15/20	6.76 ± 4.20	1,042	0,453	12	18	56,0	26,6	228	68	26,8	10,8
	CSR3-SF1	E	9/15	5.80 ± 4.30	1,049	-0,026	20	16	36,0	26,5	240	69	26,8	14,6
	CSR3-SF2	C	6/15	8.19 ± 3.97	1,042	0,395	308	1	37,4	8,0	217	61	20,9	4,8

306

Table 1: Summary of the anisotropy of magnetic susceptibility data at site level.

Columns: Locality; Site; Stage = degree of deformation from sedimentary fabric (A) to latest tectonic event (F), (*)inverse fabric and ($^{//}$)tectonic fabric parallel to the transport direction; n/N = number of specimens accepted/number of specimens measured; χ_m= mean mass magnetic susceptibility ($10^{-9}m^3kg^{-1}$) and its standard deviation; P' = corrected anisotropy degree; T = shape parameter; D = declination (°), I = inclination (°) and 95% confidence angle (°) of the principal magnetic susceptibility axes k_1 and k_3, respectively.

The SC tectonites at Sassotetto (Fig. 5) show an oblate magnetic fabric T= 0.785 ± 0.340. The magnetic foliation is SW-dipping and steeply inclined. Two different subfabrics have been detected: i. subfabric 1 is characterized by a lower anisotropy degree and higher χ_m (Table 1; Fig.4A). The magnetic fabric is slightly oblate with a N-S trending magnetic lineation; ii. subfabric 2, characterized by higher P' and lower χ_m, shows an oblate fabric with a sub-horizontal NW-SE-trending k_1 axis.

Both sites from Monastero (Fig. 5) show two overlapping magnetic fabrics. Site MSC1 is characterized by a steep WSW-dipping magnetic foliation and k_1 axis N-S trending. The plot of χ_m versus P' reveals two clusters corresponding to two subfabrics with consistent magnetic foliation and lineation (Fig. 4B, Fig. 5): i. subfabric 1 (MSC1-Sf1) is characterized by lower P' and χ_m values, and a higher dispersion of k_1 and k_2 axes on the magnetic foliation plane; ii. instead, subfabric 2 (MSC1-Sf2) shows well grouped axes.

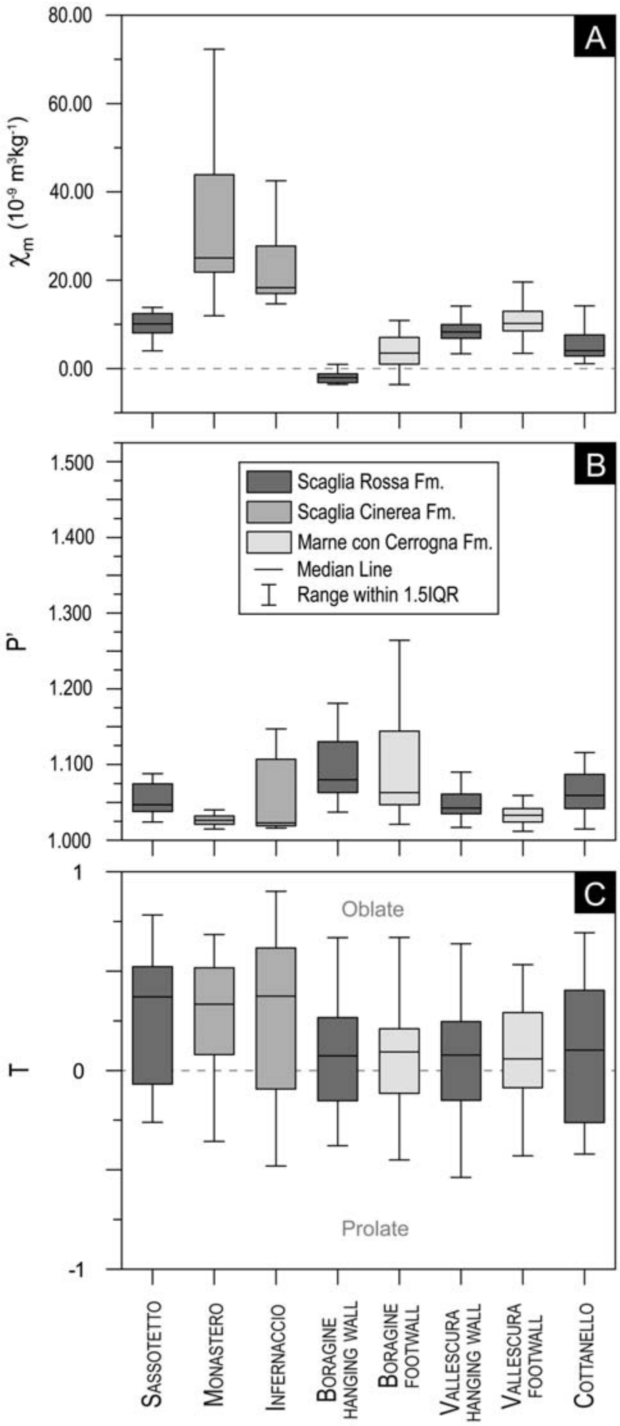

Figure 3: Box-and-whisker plots of the a) mass magnetic susceptibility (χ_m), b) corrected anisotropy degree (P') and c) shape parameter (T) for the studied localities. Central boxes include values between the lower and upper quartiles. Different gray shades correspond to different lithologies.

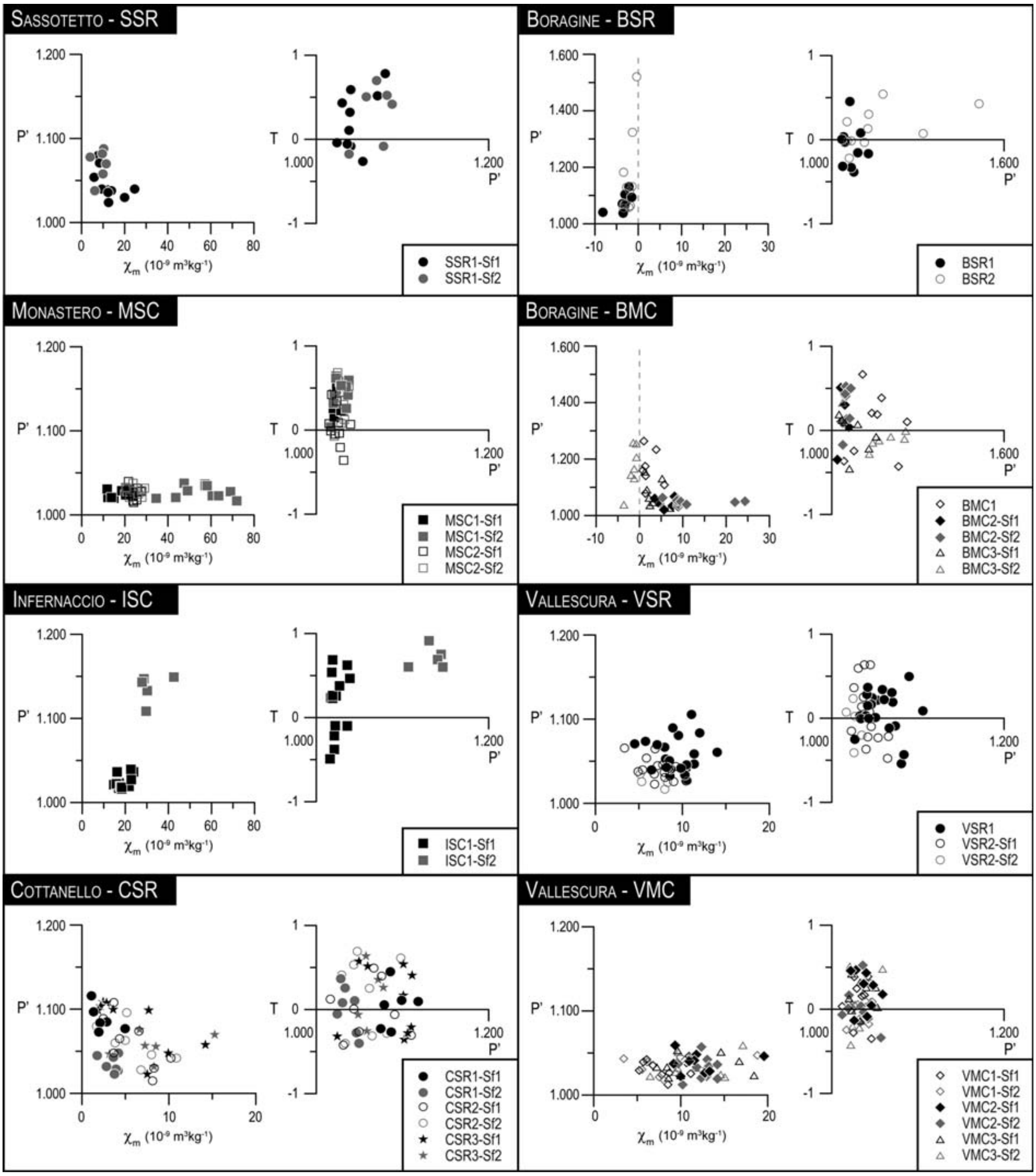

Figure 4: Corrected anisotropy degree (P') vs. mass susceptibility (χ_m) and shape parameter (T) vs. corrected anisotropy degree (P') plots for the various localities. Different symbols correspond to different lithologies: circles and stars for Scaglia Rossa Fm., squares for Scaglia Cinerea Fm. and lozenges and triangles for Marne con Cerrogna Fm.

Site MSC2 displays a sub-horizontal S-dipping magnetic foliation. Here, the two subfabrics (see MSC2-Sf1 and MSC2-Sf2 in Fig. 5) show consistent k_3 but different mean k_1 and k_2 axes orientations. The different axes orientation is associated with variations in shape parameter (T). Subfabric 1 is characterized by a slightly oblate ellipsoid (T = 0.158 ± 0.230) and a sub-horizontal E-W trending magnetic lineation, while sufabric 2, showing a N-S trending magneticlineation, is neutral with T = 0.052 ± 0.240.

Infernaccio shows the superposition of two subfabrics (see ISC1-Sf1 and ISC1-Sf2 in Fig. 5 and Fig. 4C) that differ in terms of AMS scalar parameters and k_1 axes orientations: i. subfabric 1 displays a neutral fabric with dispersed k_1 and k_2 axes and a sub-horizontal magnetic lineation mainly N-S trending, lower P' values and high variability of shape parameter ranging from -0.481 to 0.678; ii. subfabric 2 is characterized by well grouped axes with E-W trending k_1, and strongly oblate fabric and high anisotropy degree.

4.2.2 AMS from the oblique thrust ramp

The magnetic fabric is represented by a blended AMS fabric, with mainly neutral to slightly oblate magnetic ellipsoid (T = 0.077 ± 0.269) (Table 1; Fig. 3). k_3 axes are mostly grouped, while k_1 and k_2 are dispersed on the magnetic foliation. The anisotropy degree is moderate with mean value of P' = 1.066 ± 0.064. χ_m values significantly vary between localities. This in turn determines the differences in magnetic fabric configuration.

Boragine is characterized by significative changes of χ_m values between lithologies. Specimens from Scaglia Rossa Fm. (sites BSR1 and BSR2 in Fig. 6 and Fig. 4E) are mainly diamagnetic, with χ_m = -1.73 ± 2.60 [x 10^{-9} m^3kg^{-1}]. The three sites from Marne con Cerrogna Fm. show higher values, with a maximum value of 24.35 [x 10^{-9} m^3kg^{-1}]. This significantly affects the configuration of the AMS fabric in this location.

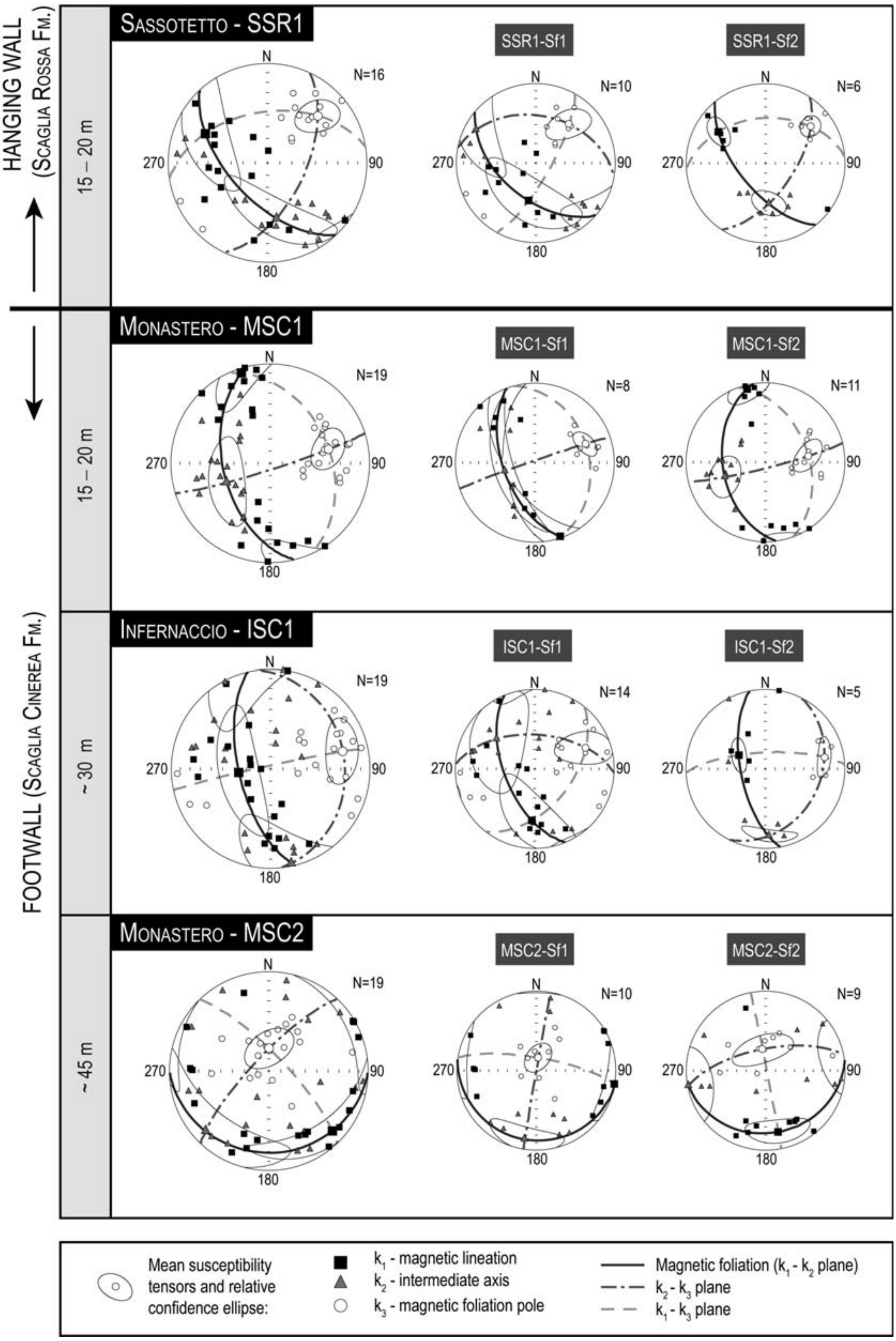

HANGING WALL (SCAGLIA ROSSA FM.)
FOOTWALL (SCAGLIA CINEREA FM.)
15 – 20 m
15 – 20 m
~ 30 m
~ 45 m
SASSOTETTO - SSR1
SSR1-Sf1
SSR1-Sf2
N=16
N=10
N=6
MONASTERO - MSC1
MSC1-Sf1
MSC1-Sf2
N=19
N=8
N=11
INFERNACCIO - ISC1
ISC1-Sf1
ISC1-Sf2
N=19
N=14
N=5
MONASTERO - MSC2
MSC2-Sf1
MSC2-Sf2
N=19
N=10
N=9
N
90
180
270
Mean susceptibility tensors and relative confidence ellipse:
k_1 - magnetic lineation
k_2 - intermediate axis
k_3 - magnetic foliation pole
Magnetic foliation (k_1 - k_2 plane)
k_2 - k_3 plane
k_1 - k_3 plane

Figure 5 (previous page): Magnetic fabric from the frontal thrust ramp at Sassotetto, Monastero (sites MSC1 and MSC2) and Infernaccio. Equal area projections in geographic coordinates of the principal magnetic susceptibility axes at site level (left) and relative subfabrics (middle and right).

Sites BSR1 and BSR2, located above the main thrust, display an E-W-trending subvertical magnetic foliation with dispersed k_1 and k_2 axes (Fig. 6). Despite higher and positive χ_m values (ranging from 0.74 to 5.73 [x 10^{-9} m^3kg^{-1}] see Fig. 4E-F), site BMC1 from Marne con Cerrogna shows a similar blended fabric with a sub-vertical E-W-trending magnetic foliation. Here, specimens display k_1 axes E-W to SW-NE trending at medium angles.

The other two sites from Marne con Cerrogna Fm., BMC2 and BMC3, are characterized by a fabric with a sub-horizontal magnetic foliation. The ellipsoid shapes are slightly oblate and prolate, respectively. The site BMC2 might be characterized by the presence of two neutral subfabrics with the same orientation of the magnetic foliation. The k_1 axes form an angle of about 122° between subfabrics. Instead, at site BMC3 specimens with negative χ_m values (BMC3-Sf1 in Fig. 6) define a prolate subfabric characterized by higher P'.

All sites from Vallescura have a consistent magnetic fabric (Fig. 7). Overall, the AMS fabric shows a magnetic foliation SW-dipping at low angle with slightly dispersed k_1 and k_2 axes. The P' values are moderate (P' = 1.040 ± 0.017) and the shape parameter is slightly oblate with mean values T = 0.283 ± 0.264 (Fig. 4G-H).

Two different subfabrics are detected at sites level: i. subfabric 1, characterized by a magnetic foliation SW-dipping and sub-horizontal SW-NE to WSW-ENE trending magnetic lineation; ii. subfabric 2 shows a sub-horizontal magnetic foliation and NW-SE to N-S trending k_1 axes.

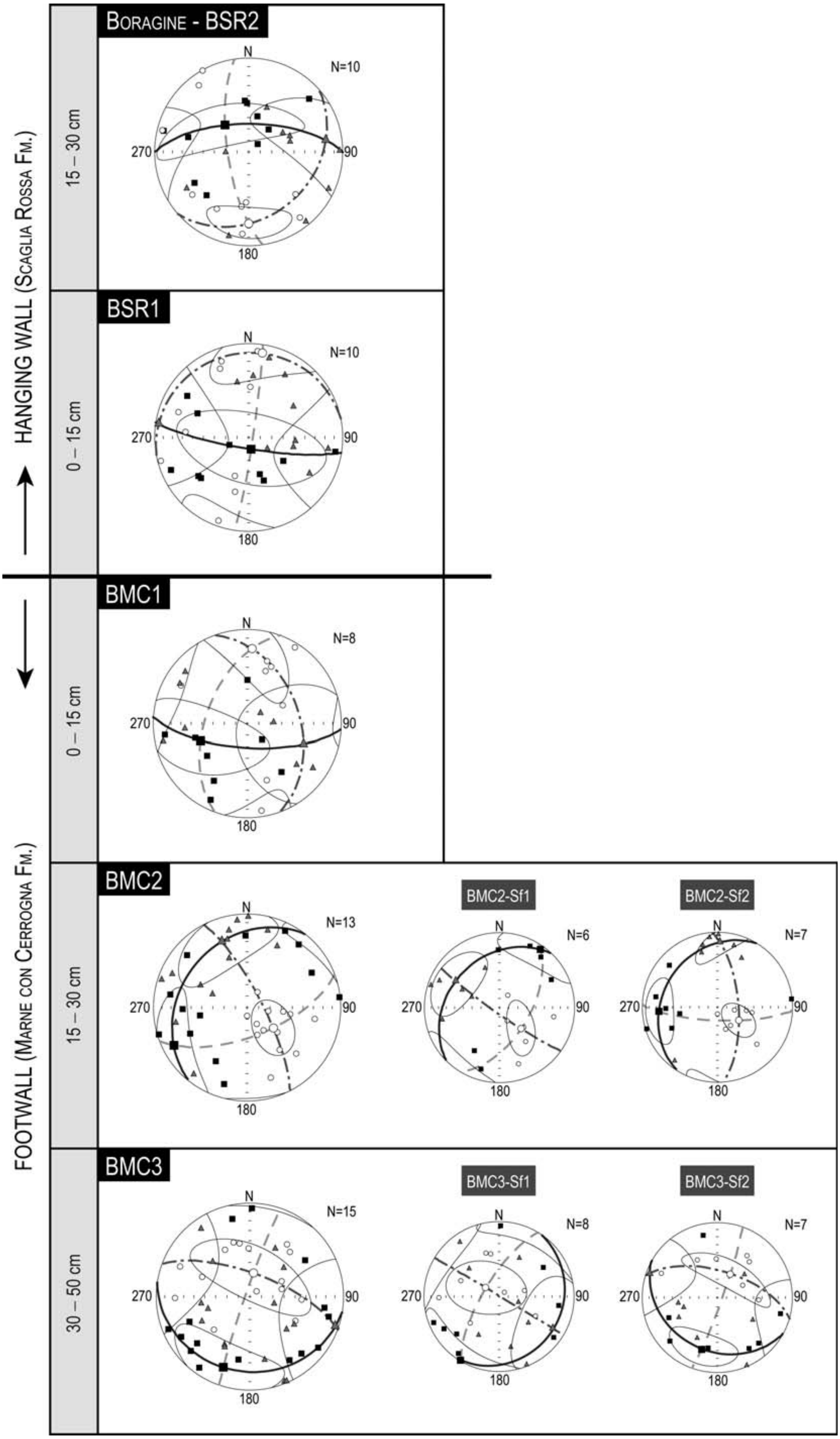
HANGING WALL (SCAGLIA ROSSA FM.)
FOOTWALL (MARNE CON CERROGNA FM.)
15 – 30 cm
0 – 15 cm
0 – 15 cm
15 – 30 cm
30 – 50 cm
BORAGINE - BSR2
N=10
BSR1
N=10
BMC1
N=8
BMC2
N=13
BMC2-Sf1
N=6
BMC2-Sf2
N=7
BMC3
N=15
BMC3-Sf1
N=8
BMC3-Sf2
N=7
N
90
180
270

388

Figure 6 (previous page): Magnetic fabric from the oblique thrust ramp at Boragine. Equal area projections in geographic coordinates of the principal magnetic susceptibility axes at site level (left) and relative subfabrics when detected (middle and right). Legend as in Figure 5.

The subfabric 1 dominates the main fabric. In fact, it strongly affects the orientation of both magnetic foliation and lineation. Furthermore, k_1 and k_3 axes show counterclockwise (CCW) and clockwise (CW) rotations when the distance from the main thrust increases, in the hanging wall and footwall respectively. Instead, subfabric 2 shows consistent configuration close to the main thrust with a NW-SE-trending magnetic lineation. In the footwall, k_1 rotates by 116° CCW passing from site VMC1 to VMC2, thus when increasing the distance from the thrust.

4.2.3 AMS from back-thrust

All sites show a magnetic fabric characterized by slightly clustered k_3 axes. The k_1 and k_2 axes are dispersed on the N to NNE-dipping magnetic foliation. The low to moderate χ_m (mean value of 5.26 ± 3.37 [x 10^{-9} m^3kg^{-1}]) and P' values are consistent among sites (Tab. 1; Fig. 4D). Shape parameters change from mainly oblate at site CSR3 to slightly prolate at sites CSR1. At the same time, the magnetic foliation shifts from sub-horizontal to sub-vertical (Fig. 8).

In addition, all sites reveal the presence of two subfabrics: i. subfabric 1 showing a slightly inclined magnetic lineation NNW to NE trending; ii. subfabric 2 characterized by a NW-SE-trending sub-horizontal magnetic lineation. Similar fabric has been previously documented in this area (Mattei et al., 1995).

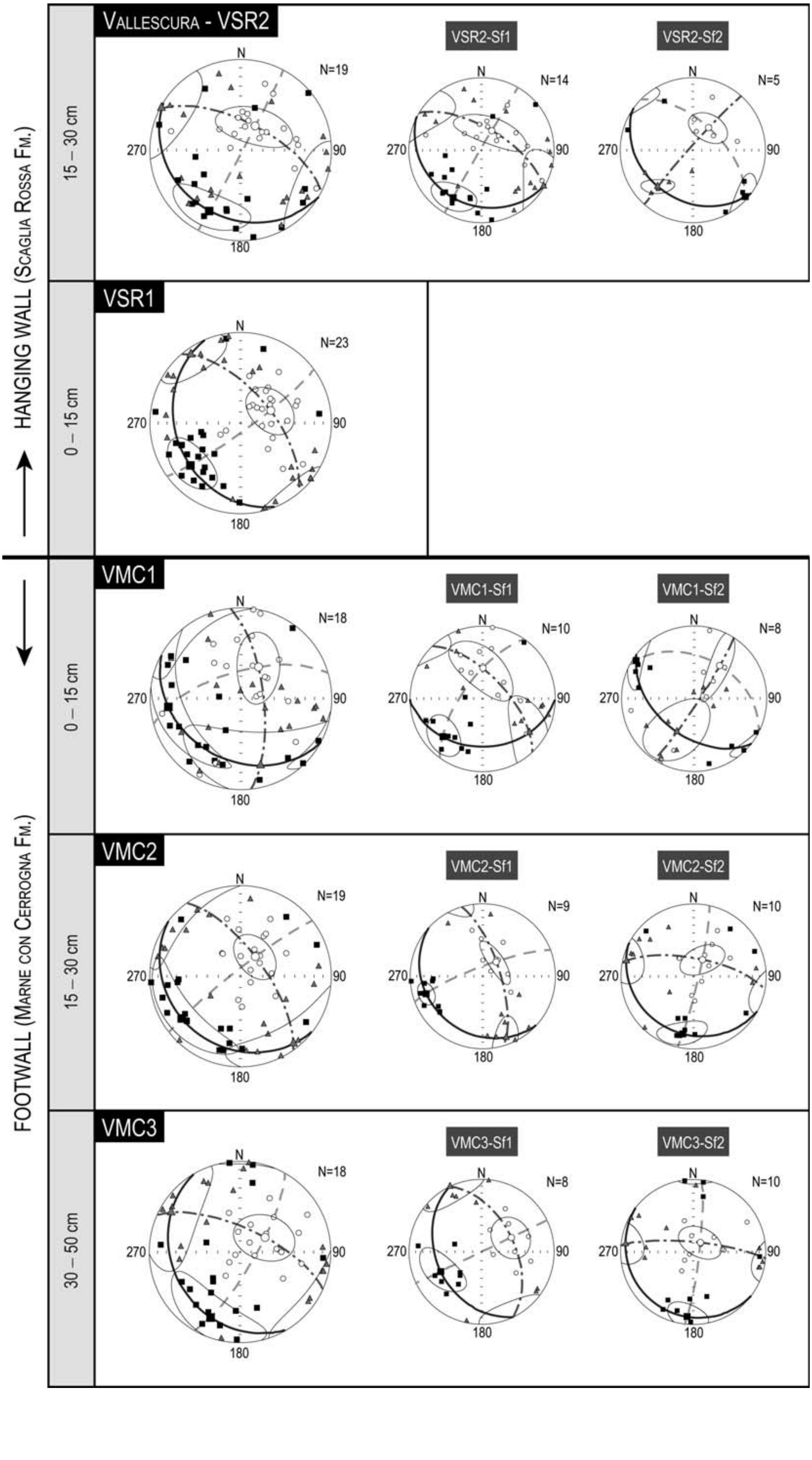
VALLESCURA - VSR2
VSR2-Sf1
VSR2-Sf2
N=19
N=14
N=5
VSR1
N=23
VMC1
VMC1-Sf1
VMC1-Sf2
N=18
N=10
N=8
VMC2
VMC2-Sf1
VMC2-Sf2
N=19
N=9
N=10
VMC3
VMC3-Sf1
VMC3-Sf2
N=18
N=8
N=10
N
270
90
180
15 – 30 cm
0 – 15 cm
30 – 50 cm
HANGING WALL (SCAGLIA ROSSA FM.)
FOOTWALL (MARNE CON CERROGNA FM.)

409

Figure 7 (previous page): Magnetic fabric from the oblique thrust ramp at Vallescura. Equal area projections in geographic coordinates of the principal magnetic susceptibility axes at site level (left) and relative subfabrics when detected (middle and right). Legend as in Figure 5.

A closer look reveals the dominance of Subfabric 1 on the main fabric in proximity to the main thrust (site CSR1). The subfabric 2 progressively becomes dominant on the definition of the magnetic foliation with the increment of the distance from the fault (Fig. 8). Particularly, variations in the Subfabric 1 configuration control the rotation of k_1 and k_2 axes. In fact, from site CSR3 to CSR1 the progressive verticalization of the magnetic foliation is associated with a CCW rotation of k_1 axis from N20° to NNW. On the contrary, in all sites the subfabric 2 shows stable NW-SE trending orientation of the magnetic lineation. In these cases, k_1 acts as a rotation pin producing a progressive switch between k_3 and k_2 axes and the verticalization of the magnetic foliation when getting closer to the main thrust.

5. Comparison with structural data

Magnetic fabric analysis revealed straightforward correlations with structural data. It was possible to infer 6 different AMS fabrics, named from A to F according to the intensity of deformation; symbols * and $^{//}$ indicate inverse fabric and parallelism with transport direction, respectively.

In the following, we report the comparison between AMS and structural data at site level.

At Sassotetto, subfabric 1 is represented by a magnetic foliation parallel to the pressure solution cleavage, where k_1 is close to the direction of the slip vector. This subfabric may represent an

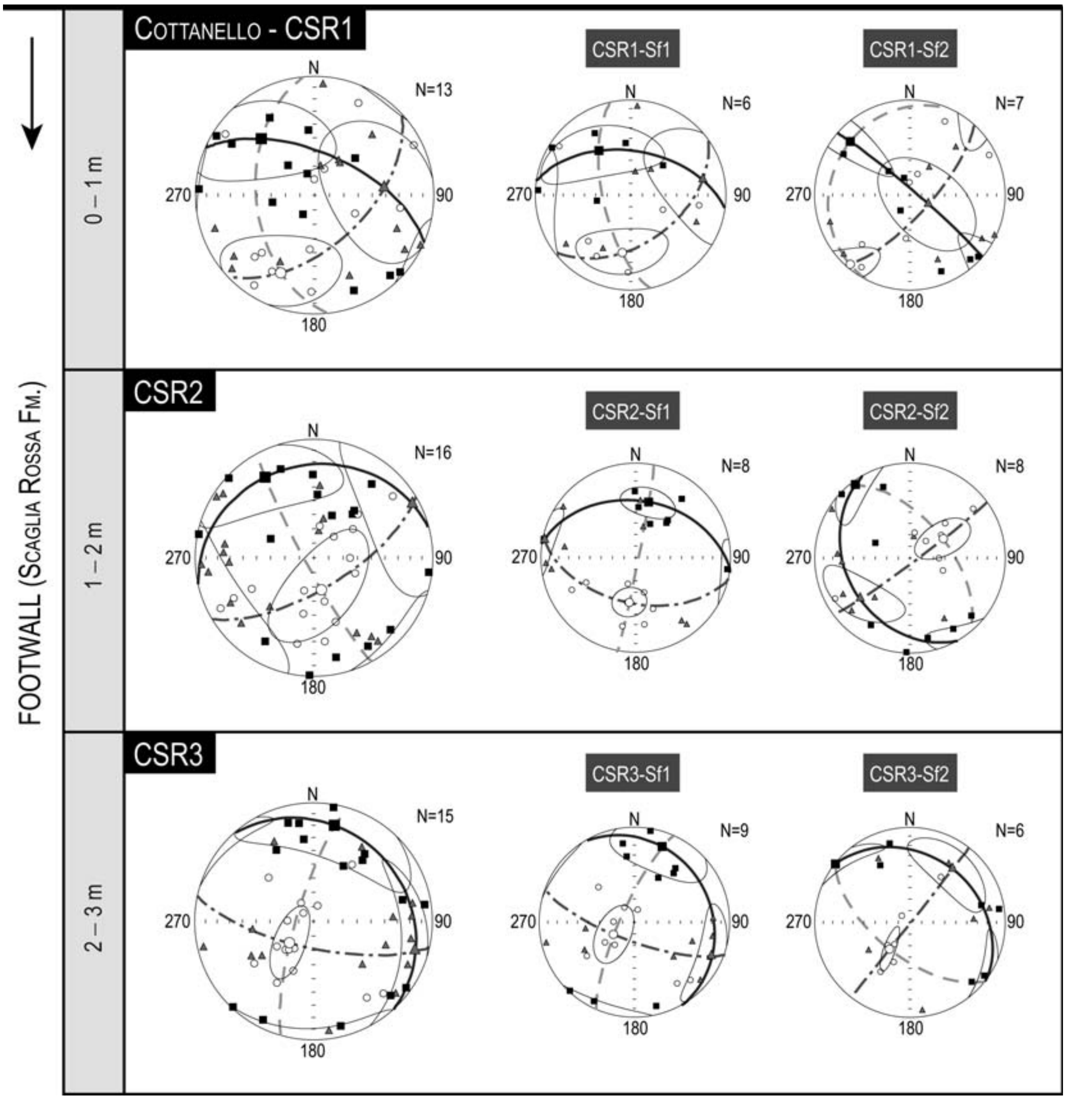

Figure 8: Magnetic fabric from the back-thrust at Cottanello. Equal area projections in geographic coordinates of the principal magnetic susceptibility axes at site level (left) and relative subfabrics (middle and right). Legend as in Figure 5.

---

advanced stage of deformation with k_1 parallel to the transport direction (Stage E, Fig. 9). In the same locality, subfabric 2 shows k_1 and k_3 consistent with S/C intersection and S pole, respectively. It represents the early stage of shearing with k_1 at the S/C intersection (Stage C,

Fig. 9).

At Monastero, a different magnetic fabric is documented in sites MSC1 and MSC2, sampled at 15 m and 45 m from the main thrust, respectively. In site MSC1, k_1 is at the S/C intersection and the magnetic foliation is parallel to the S plane. In particular, subfabric 1 reveals the coincidence between k_3 and S pole, but k_1 axes are dispersed in the foliation plane parallel to S. Subfabric 2, instead, reveals a better clustering of k_1, aligned with the S/C intersection. Here, the two subfabrics may represent the same process of earlier deformation stages (Stage C) with a better definition of the tectonic fabric in subfabric 2 due to higher χ_m values.

In site MSC2, subfabric 1 shows an horizontal magnetic foliation consistent with the bedding and moderate dispersion of k_1 and k_2 axis, representing the preserved sedimentary fabric of the Scaglia Cinerea Fm. (Stage A, Fig. 9). In subfabric 2, k_2 and k_3 are dispersed on a girdle and k_1 is at the S/C intersection. This configuration might represent the early stage of deformation (Stage B), where the sedimentary fabric is partially preserved and k_1 corresponds to the intersection lineation between bedding and cleavage. In fact, in incipient deformation stage the magnetic foliation remains parallel to the bedding while the magnetic lineation becomes perpendicular to the bedding-parallel shortening. When the deformation increases the magnetic foliation poles create a girdle parallel to the shortening (Hrouda and Chadima, 2019). Furthermore, principal axes of maximum susceptibility are particularly sensitive to tectonic shortening, as they develop a magnetic lineation that mimics the intersection of bedding and tectonic flattening plane (Parés, 2015).

At Infernaccio, the subfabric 1 shows the parallelism between magnetic foliation and S plane, and k_1 is moving toward the slip vector direction (Stage D, Fig. 9). On the contrary, subfabric 2 reveals k_1 axes at high angle in respect to the S/C intersection and sub-parallel to the slip vector (Stage E, Fig. 9).

Where the magnetic lineation is mainly defined by paramagnetic carriers, it evolves from parallelism to the S/C intersection during earlier deformational stages to parallelism to the slip vector in advanced stages (Parés et al., 1999; Pueyo Anchuela et al., 2010).

The configuration of the subfabric 1 is consistent between Sassotetto and Infernaccio, differing only by 24° in the magnetic foliation orientation. Instead, the subfabric 2 shows an increment in k_1 axis inclination. On the contrary, at Monastero a change in magnetic foliation dipping angle is visible in both subfabrics. Particularly, subfabric 1 shows a 61° CW rotation of the magnetic lineation associated with the verticalization of the magnetic foliation from site MSC1 to site MSC2. In both sites, the subfabric 2 shows a consistent sub-horizontal N-S trending magnetic lineation. Only an increment in the magnetic foliation dipping is here visible.

Overall, the simple-shear-dominated deformation regime (Calamita et al., 2012) from the frontal ramp shows a magnetic foliation parallel to the S or in between S and C planes and k_1 parallel to the S/C intersection or to the slip vector, depending on the degree of deformation (from Stage C to E). Sedimentary features and early stage of cleavage development are also visible at site MSC2 (45 m from the thrust).

A similar behaviour is documented at Cottanello, where all 3 sites show a magnetic foliation with an intermediate orientation between S and C planes and k_1 axes dispersed from the S/C intersection toward the slip vector (inferred from the S/C intersection). A magnetic foliation at an intermediate position between S and C planes was previously described in other fault zones, both under extensional and compressional regimes (Aranguren et al., 1996; Casas-Sainz et al., 2017). Such relationships can be explained by both deformational and mineralogical controls (Casas-Sainz et al., 2018).

Particularly at site CSR1, the subfabric 1 shows a magnetic foliation parallel to the S and slightly dispersion of k_1 between the S/C intersection and the slip vector (Stage D in Fig.9). At sites CSR2 and CSR3, it shows a magnetic foliation parallel to the C and k_1 consistent with the inferred slip vector (Stage E).

In all sites, subfabric 2 shows a parallelism between k_1 and the S/C intersection (Stage C), representing the intersection lineation, while the magnetic foliation is characterized by the same strike of C plane, but variable dipping angles. In fact, at site CSR1, k_2 and k_3 are dispersed on a girdle, while at site CSR3 the magnetic foliation shows an intermediate orientation between S and C planes. On the contrary, site CSR2 shows a SW dipping magnetic foliation.

The sub-simple shear of Cottanello (Pace et al., 2015) shows a magnetic foliation intermediate between S and C, k_1 parallel to the S/C intersection or the slip vector, depending on the degree of deformation witnessed by groups of specimens.

At Vallescura and Boragine, the sampling was done across the thrust plane, both in the hanging-wall and footwall block.

In the hanging-wall block of Vallescura, site VSR1 and subfabric 1 of VSR2 show the magnetic foliation consistent with the S plane and k_1 parallel to the transport direction (Stage $E^{//}$, Fig.9). The subfabric 2 of site VSR2 reveals a k_1 axis coincident with the E-E’ intersection (Stage F, Fig. 9).

In the footwall block, also VMC1 magnetic fabric shows a parallelism between magnetic foliation and S plane. The subfabric 1 is characterized by a fan dispersion of k_2 and k_3 and k_1 parallel to the transport direction (Stage $E^{//}$), while subfabric 2 reveals k_1 axis parallel to the E-E’ intersection (Stage F). In both VMC2 e VMC3 the subfabric 1 is characterized by the parallelisms between magnetic foliation and S planes, and k_1 is grouped in an intermediate orientation between the S/T intersection and the transport direction (Stage $D^{//}$). On the contrary, in both sites subfabric 2 shows a parallelism between magnetic foliation planes and S planes. k_1 axes are N-S trending and may indicate a parallelism with the inferred slip vector (Stage

$E^{(//)}$).

At Boragine most sites show low bulk magnetic susceptibility values (k_m), close to the instrumental limit. This might have caused problems related to mean tensors and their confidence ellipses calculation. For that reason, only site BMC2, characterized by high χ_m values, is considered reliable for further interpretations. However, for the sake of completeness, we reported the comparison between AMS and structural data for all sites.

In the hanging wall, sites BSR1 and BSR2 show highly scattered axes, with k_1 mostly subvertical and dispersed on a E-W girdle. In both sites k_3 is partially grouped at the E-E' intersection (Stage F*). At site BMC1, k_2 and k_3 axes are highly dispersed along a N-S girdle, while k_1 axes are grouped in the transport direction (Stage $E^{//}$).

At site BMC2, the subfabric 1 shows a magnetic foliation intermediate between S and T planes and k_1 has a double tendency to parallelize with the direction of the slip vector and the transport direction (Stage E or $E^{//}$ in Fig. 9). The subfabric 2 is characterized by a magnetic foliation parallel to S planes and k_1 intermediate between S/T intersection and the slip vector (Stage $D^{//}$, Fig. 9).

Finally, in BMC3, subfabric 1 shows a subhorizontal magnetic foliation with interdispersed k_2 and k_3 axes, while k_1 are mostly grouped with double tendency in the slip vector and the transport directions. Subfabric 2 shows high dispersed k_1 and k_2 axes, while k_3 is grouped at high angle from N to E. The fabric is inverse and k_3 might be considered to assume an orientation intermediate between the directions of the slip vector and the inferred slip vector.

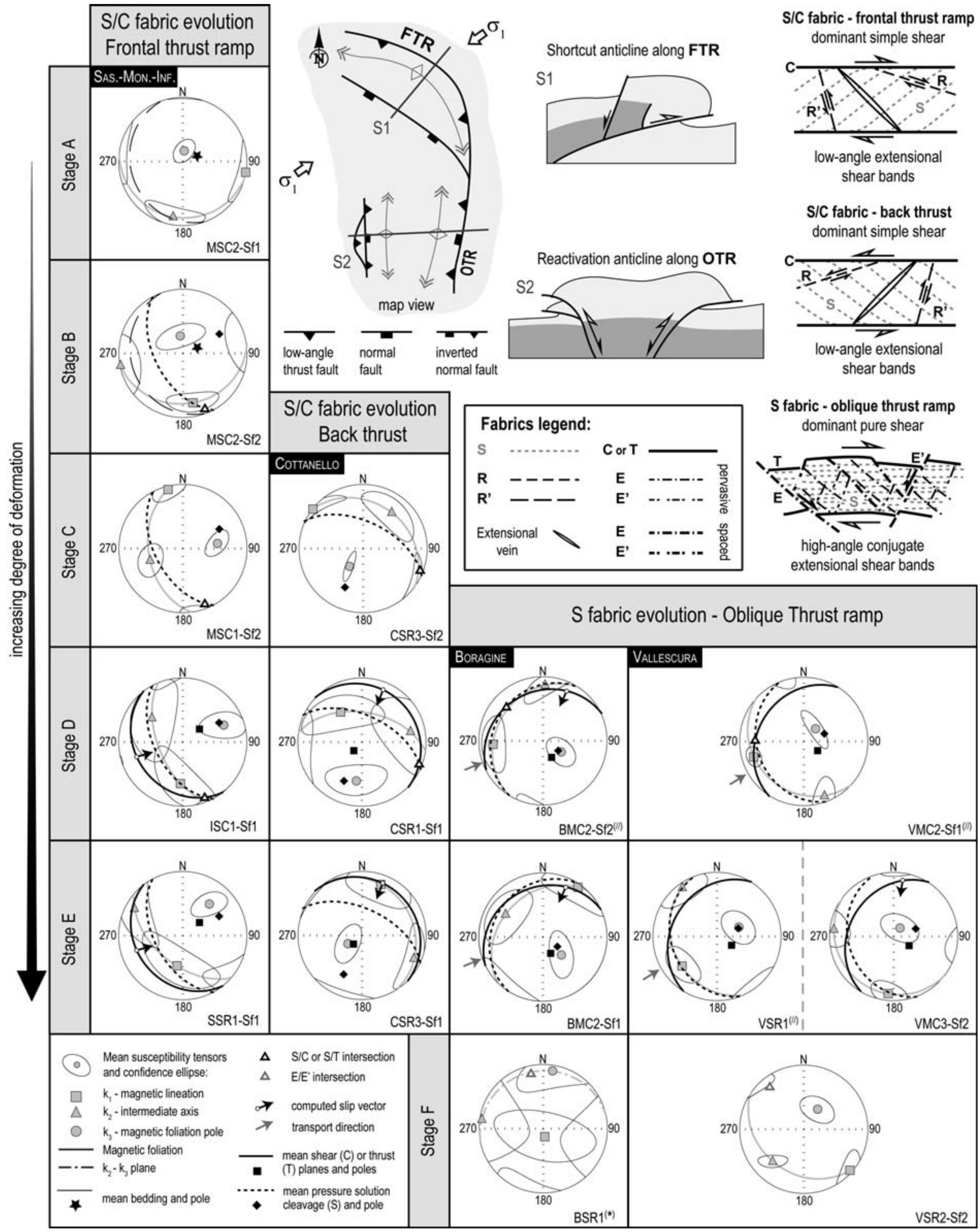

Figure 9: Summary of magnetic fabric stages and comparison with structural data. Representative examples from the different deformation regimes are reported. Conceptual diagram of the different types of shear deformation fabric (ZX section of strain ellipses) related

to frontal (FTR) and oblique (OTR) thrust ramps (modified from Calamita et al., 2012; Pace et al., 2015).

In this pure-shear-dominated deformation regime (Calamita et al., 2012) the magnetic foliation is mostly parallel to S, even if some sites from Boragine show additional complexities where k_1 (or k_3 in case of possible inverse fabric) are: i. parallel to the slip vector (Stage E or E*); ii. parallel to the transport direction (Stage $E^{//}$); iii. in between the S/T intersection and the slip vector (Stage $D^{//}$ or D*); iv. parallel to the E-E' intersection close to the main thrust (Stage F or F*).

6. Conclusion

We investigated the magnetic anisotropy in shear zones from 3 sectors of the Northern Apennines fold-and-thrust belt, characterized by different combinations of simple and pure shear (Calamita et al., 2012; Pace et al., 2015): the OAS frontal thrust ramp, the OAS oblique ramp and an inner sector characterized by a back-thrust in a transpressive context.

The documented magnetic fabric shows similar evolution in all the deformation regimes, depending upon the increasing of deformation (lower vorticity number) and proximity to the main thrust (Fig. 9). Six different fabrics were identified:

A. sedimentary fabric characterized by magnetic foliation-bedding parallelism (Hrouda and Chadima, 2019 and references therein);

B. an early stage of deformation with k_1 at the intersection between bedding and S plane (so called intersection lineation; Hrouda and Chadima, 2019);

C. magnetic foliation parallel to S and k_1 parallel to the S/C intersection, progressively evolving with the deformation increments (Parés et al., 1999; Pueyo Anchuela et al., 2010) in stage D;

D. magnetic foliation parallel to S and k_1 (or k_3 in case of possible inverse fabrics documented in Boragine) intermediate between S/C intersection and the slip vector. In case of pure-shear-dominated regime, k_1 is intermediate between S/T intersection and the transport direction;

E. the magnetic foliation shows a double tendency to parallelize either the S or the C planes, and k_1 is parallel to the slip vector or the transport direction (in case of pure shear component);

F. documented in pure-shear-dominated deformation regime only, shows the parallelism between k_1 (or k_3 in case of possible inverse fabrics) axis and extensional planes intersection.

These results show that the magnetic fabric is more sensitive to the simple shear deformation, as the magnetic lineation tends to parallelize mostly with the computed slip vector. In pure-shear dominated regimes, the magnetic lineation becomes parallel to the transport direction when the deformation is really intense (sites at less than 15-30 cm from the thrust plane).

These results suggest that it is fundamental to use a combination of density diagrams and cluster analysis on AMS data in order to discriminate subfabrics linked to different events. In this way, AMS potential as a tool to unravel different sedimentary or tectonic features is enhanced.

Acknowledgments

CRT, ET, EZ and SS were funded by MIUR ex-60% attributed to SS and EZ. DS Erasmus traineeship at CIMaN - ALP was funded by University of Silesia in Katowice.

Supplementary material

Supplementary Table 1: Anisotropy of magnetic susceptibility data at specimen level of all the studied sites, subdivided by locality. Columns: Site; Specimen name; k_m = mean bulk magnetic susceptibility (µSI); weight (g); χ_m = mean mass magnetic susceptibility (10^{-9} m^3kg^{-1}); L = magnetic lineation; F = magnetic foliation; P' = corrected anisotropy degree; T = shape parameter; ; D = declination (°), I = inclination (°) of the principal magnetic susceptibility axes k_1, k_2 and k_3, respectively.

Supplementary Table 2: Anisotropy of magnetic susceptibility data at site level for all the studied localities. Columns: Locality; Site; Stage = degree of deformation from sedimentary fabric (A) to latest tectonic event (F), (*) inverse fabric and (//) tectonic fabric parallel to the transport direction; n/N = number of specimens accepted/number of specimens measured; k_m = mean bulk magnetic susceptibility (µSI) and its standard deviation; χ_m = mean mass magnetic susceptibility (10^{-9} m^3kg^{-1}) and its standard deviation; L = magnetic lineation; F = magnetic foliation; P' = corrected anisotropy degree; T = shape parameter; D = declination (°), I = inclination (°) and 95% confidence angle (°) of the principal magnetic susceptibility axes k_1, k_2 and k_3, respectively.

References

Alberti, M., Decandia, F.A., Tavarnelli, E., 1996. Modes of propagation of the compressional deformation in the Umbria-Marche Apennines. Memorie della Società Geologica Italiana 51, 71–82.

Alfonsi, L., 1995. Wrench tectonic in Central Italy, a segment of the Sabina Fault. Bollettino della Società Geologica Italiana 114, 411–421.

Almqvist, B.S.G., Koyi, H., 2018. Bulk strain in orogenic wedges based on insights from magnetic fabrics in sandbox models. Geology 46, 483–486. https://doi.org/10.1130/G39998.1

Aranguren, A., Cuevas, J., Tubía, J.M., 1996. Composite magnetic fabrics from S-C mylonites. Journal of Structural Geology 18, 863–869. https://doi.org/10.1016/0191-8141(96)00013-2

Arthur, M.A., Fischer, A.G., 1977. Upper Cretaceous–Paleocene magnetic stratigraphy at Gubbio, Italy I. Lithostratigraphy and sedimentology. GSA Bulletin 88, 367–371. https://doi.org/10.1130/0016-7606(1977)88<367:UCMSAG>2.0.CO;2

Aubourg, C., Smith, B., Eshraghi, A., Lacombe, O., Authemayou, C., Amrouch, K., Bellier, O., Mouthereau, F., 2010. New magnetic fabric data and their comparison with palaeostress markers in the Western Fars Arc (Zagros, Iran): tectonic implications. Geological Society, London, Special Publications 330, 97–120. https://doi.org/10.1144/SP330.6

Berthé, D., Choukroune, P., Jegouzo, P., 1979. Orthogneiss, mylonite and non coaxial deformation of granites: the example of the South Armorican Shear Zone. Journal of Structural Geology 1, 31–42. https://doi.org/10.1016/0191-8141(79)90019-1

Boccaletti, M., Calamita, F., Viandante, M.G., 2005. La Neo-Catena litosferica appenninica nata a partire dal Pliocene inferiore come espressione della convergenza Africa-Europa. Bollettino della Società Geologica Italiana 124, 87–105.

Borradaile, G.J., Alford, C., 1988. Experimental shear zones and magnetic fabrics. Journal of Structural Geology 10, 895–904. https://doi.org/10.1016/0191-8141(88)90102-2

Borradaile, G.J., Hamilton, T., 2004. Magnetic fabrics may proxy as neotectonic stress trajectories, Polis rift, Cyprus. Tectonics 23. https://doi.org/10.1029/2002TC001434

Borradaile, G.J., Henry, B., 1997. Tectonic applications of magnetic susceptibility and its anisotropy. Earth-Science Reviews 42, 49–93. https://doi.org/10.1016/S0012-8252(96)00044-X

Borradaile, G.J., Jackson, M., 2004. Anisotropy of magnetic susceptibility (AMS): magnetic petrofabrics of deformed rocks. Geological Society, London, Special Publications 238, 299–360. https://doi.org/10.1144/GSL.SP.2004.238.01.18

Borradaile, G.J., Jackson, M., 2010. Structural geology, petrofabrics and magnetic fabrics (AMS, AARM, AIRM). Journal of Structural Geology 32, 1519–1551. https://doi.org/10.1016/j.jsg.2009.09.006

Butler, R.W.H., Tavarnelli, E., Grasso, M., 2006. Structural inheritance in mountain belts: An Alpine–Apennine perspective. Journal of Structural Geology, Tectonic inversion and structural inheritance in mountain belts 28, 1893–1908. https://doi.org/10.1016/j.jsg.2006.09.006

Calamita, F., 1991. Extensional mesostructures in thrust shear zones examples from the Umbro-Marchean Apennines. Bollettino della Società Geologica Italiana 110, 649–660.

Calamita, F., Coltorti, M., Piccinini, D., Pierantoni, P.P., Pizzi, A., Ripepe, M., Scisciani, V., Turco, E., 2000. Quaternary faults and seismicity in the Umbro-Marchean Apennines

(Central Italy): evidence from the 1997 Colfiorito earthquake. Journal of Geodynamics 29, 245–264. https://doi.org/10.1016/S0264-3707(99)00054-X

Calamita, F., Decandia, F.A., Deiana, G., Fiori, A.P., 1991. Deformation of SC tectonites in the Scaglia Cinera Formation in the Spoleto area (Southeast Umbria). Bollettino della Società Geologica Italiana 110, 661–665.

Calamita, F., Deiana, G., Invernizzi, C., Mastrovincenzo, S., 1987. Analisi strutturale della «Linea Amona-Anzio» Auct. tra Cittareale e Micigliano (Rieti). Bollettino della Società Geologica Italiana 106, 365–375.

Calamita, F., Satolli, S., Scisciani, V., Esestime, P., Pace, P., 2011. Contrasting styles of fault reactivation in curved orogenic belts: Examples from the Central Apennines (Italy). GSA Bulletin 123, 1097–1111. https://doi.org/10.1130/B30276.1

Calamita, F., Satolli, S., Turtù, A., 2012. Analysis of thrust shear zones in curve-shaped belts: Deformation mode and timing of the Olevano-Antrodoco-Sibillini thrust (Central/Northern Apennines of Italy). Journal of Structural Geology 44, 179–187. https://doi.org/10.1016/j.jsg.2012.07.007

Caricchi, C., Cifelli, F., Kissel, C., Sagnotti, L., Mattei, M., 2016. Distinct magnetic fabric in weakly deformed sediments from extensional basins and fold-and-thrust structures in the Northern Apennine orogenic belt (Italy). Tectonics 35, 238–256. https://doi.org/10.1002/2015TC003940

Casas-Sainz, A.M., Gil-Imaz, A., Simón, J.L., Izquierdo-Llavall, E., Aldega, L., Román-Berdiel, T., Osácar, M.C., Pueyo-Anchuela, Ó., Ansón, M., García-Lasanta, C., Corrado, S., Invernizzi, C., Caricchi, C., 2018. Strain indicators and magnetic fabric in intraplate fault zones: Case study of Daroca thrust, Iberian Chain, Spain. Tectonophysics 730, 29–47. https://doi.org/10.1016/j.tecto.2018.02.013

Casas-Sainz, A.M., Román-Berdiel, T., Oliva-Urcia, B., García-Lasanta, C., Villalaín, J.J., Aldega, L., Corrado, S., Caricchi, C., Invernizzi, C., Osácar, M.C., 2017. Multidisciplinary approach to constrain kinematics of fault zones at shallow depths: a case study from the Cameros–Demanda thrust (North Spain). Int J Earth Sci (Geol Rundsch) 106, 1023–1055. https://doi.org/10.1007/s00531-016-1349-5

Castellarin, A., Colacicchi, R., Praturlon, A., Cantelli, C., 1982. The Jurassic-Lower Pliocene history of the Ancona-Anzio Line (Central Italy). Mem. Soc. Geol. Ital 24, 325–336.

Centamore, E., Micarelli, A., 1991. L'ambiente fisico delle Marche. Geologia, Geomorfologia, Idrogeologia (scala 1: 100. 000).

Chadima, M., Jelínek, V., 2008. Anisoft 4.2.–Anisotropy data browser. Contributions to Geophysics and Geodesy 38, 38–41.

Ciarapica, G., Passeri, L., 2002. The palaeogeographic duplicity of the Apennines. Boll. Soc. Geol. It. 1, 67–75.

Di Domenica, A., Turtù, A., Satolli, S., Calamita, F., 2012. Relationships between thrusts and normal faults in curved belts: New insight in the inversion tectonics of the Central-Northern Apennines (Italy). Journal of Structural Geology 42, 104–117. https://doi.org/10.1016/j.jsg.2012.06.008

Ferré, E.C., Gébelin, A., Till, J.L., Sassier, C., Burmeister, K.C., 2014. Deformation and magnetic fabrics in ductile shear zones: A review. Tectonophysics 629, 179–188. https://doi.org/10.1016/j.tecto.2014.04.008

Fossen, H., 2010. Structural Geology. Cambridge University Press. https://doi.org/10.1017/CBO9780511777806

Fossen, H., Cavalcante, G.C.G., 2017. Shear zones – A review. Earth-Science Reviews 171, 434–455. https://doi.org/10.1016/j.earscirev.2017.05.002

Ghisetti, F., 1987. Mechanisms of thrust faulting in the Gran Sasso chain, Central Apennines, Italy. Journal of Structural Geology 9, 955–967. https://doi.org/10.1016/0191-8141(87)90004-6

Graham, J.W., 1966. Significance of Magnetic Anisotropy in Appalachian Sedimentary Rocks, in: Steinhart, J.S., Smith, T.J. (Eds.), Geophysical Monograph Series. American Geophysical Union, Washington, D. C., pp. 627–648. https://doi.org/10.1029/GM010p0627

Harris, L.B., Cobbold, P.R., 1985. Development of conjugate shear bands during bulk simple shearing. Journal of Structural Geology 7, 37–44. https://doi.org/10.1016/0191-8141(85)90113-0

Holdsworth, R.E., Strachan, R.A., Alsop, G.I., Grant, C.J., Wilson, R.W., 2006. Thrust sequences and the significance of low-angle, out-of-sequence faults in the northernmost Moine Nappe and Moine Thrust Zone, NW Scotland. Journal of the Geological Society 163, 801–814. https://doi.org/10.1144/0016-76492005-076

Housen, B.A., Van Der Pluijm, B.A., Essene, E.J., 1995. Plastic behavior of magnetite and high strains obtained from magnetic fabrics in the Parry Sound shear zone, Ontario Grenville Province. Journal of Structural Geology 17, 265–278. https://doi.org/10.1016/0191-8141(94)E0045-Z

Hrouda, F., 2002. Low-field variation of magnetic susceptibility and its effect on the anisotropy of magnetic susceptibility of rocks. Geophysical Journal International 150, 715–723. https://doi.org/10.1046/j.1365-246X.2002.01731.x

Hrouda, F., Chadima, M., 2019. Examples of tectonic overprints of magnetic fabrics in rocks of the Bohemian Massif and Western Carpathians. Int J Earth Sci (Geol Rundsch). https://doi.org/10.1007/s00531-019-01786-8

Hrouda, F., Ježek, J., 1999. Magnetic anisotropy indications of deformations associated with diagenesis. Geological Society, London, Special Publications 151, 127–137. https://doi.org/10.1144/GSL.SP.1999.151.01.13

ISPRA, 2007, Carta Geologica d'Italia 1:50.000 - Catalogo delle Formazioni, *Periodici tecnici Volume 7*

Jégouzo, P., 1980. The South Armorican Shear Zone. Journal of Structural Geology, Shear zones in rocks 2, 39–47. https://doi.org/10.1016/0191-8141(80)90032-2

Jelínek, V., 1977. The statistical theory of measuring anisotropy of magnetic susceptibility of rocks and its application. Geofyzika Brno, Czech Republic.

Jelínek, V., 1981. Characterization of the magnetic fabric of rocks. Tectonophysics 79, T63–T67. https://doi.org/10.1016/0040-1951(81)90110-4

Koopman, A., 1983. Detachment tectonics in the Central Apennines, Italy. Geologica Ultraiectina 30, 1–55.

Lavecchia, G., 1985. Il sovrascorrimento dei Monti Sibillini: analisi cinematica e strutturale. Bollettino della Società Geologica Italiana 104, 161–194.

Lister, G.S., Snoke, A.W., 1984. S-C Mylonites. Journal of Structural Geology 6, 617–638. https://doi.org/10.1016/0191-8141(84)90001-4

Mattei, M., Funiciello, R., Kissel, C., 1995. Paleomagnetic and structural evidence for Neogene block rotations in the Central Apennines, Italy. J. Geophys. Res. 100, 17863–17883. https://doi.org/10.1029/95JB00864

Pace, P., Calamita, F., 2014. Push-up inversion structures v. fault-bend reactivation anticlines along oblique thrust ramps: examples from the Apennines fold-and-thrust belt (Italy). Journal of the Geological Society 171, 227–238. https://doi.org/10.1144/jgs2013-053

Pace, P., Calamita, F., Tavarnelli, E., 2015. Brittle-ductile shear zones along inversion-related frontal and oblique thrust ramps: Insights from the Central-Northern Apennines curved thrust system (Italy), in: Mukherjee, S., Mulchrone, K.F. (Eds.), Ductile Shear Zones. John Wiley & Sons, Ltd, Chichester, UK, pp. 111–127. https://doi.org/10.1002/9781118844953.ch8

Parés, J.M., 2015. Sixty years of anisotropy of magnetic susceptibility in deformed sedimentary rocks. Front. Earth Sci. 3. https://doi.org/10.3389/feart.2015.00004

Parés, J.M., van der Pluijm, B.A., 2002. Evaluating magnetic lineations (AMS) in deformed rocks. Tectonophysics 350, 283–298. https://doi.org/10.1016/S0040-1951(02)00119-1

Parés, J.M., van der Pluijm, B.A., Dinarès-Turell, J., 1999. Evolution of magnetic fabrics during incipient deformation of mudrocks (Pyrenees, northern Spain). Tectonophysics 307, 1–14. https://doi.org/10.1016/S0040-1951(99)00115-8

Passchier, C.W., 2001. Flanking structures. Journal of Structural Geology 23, 951–962. https://doi.org/10.1016/S0191-8141(00)00166-8

Pierantoni, P.P., 1996. Faglie trascorrenti sin-thrusting come ripartizione della deformazione: L'esempio della Faglia Sabina (Appennino Centrale). Studi Geologici Camerti 14, 279–289.

Platt, J.P., 1984. Secondary cleavages in ductile shear zones. Journal of Structural Geology 6, 439–442. https://doi.org/10.1016/0191-8141(84)90045-2

Platt, J.P., Vissers, R.L.M., 1980. Extensional structures in anisotropic rocks. Journal of Structural Geology 2, 397–410. https://doi.org/10.1016/0191-8141(80)90002-4

Ponce de Leon, M.I., Choukroune, P., 1980. Shear zones in the iberian arc. Journal of Structural Geology, Shear zones in rocks 2, 63–68. https://doi.org/10.1016/0191-8141(80)90035-8

Pueyo Anchuela, Ó., Pocoví Juan, A., Gil Imaz, A., 2010. Tectonic imprint in magnetic fabrics in foreland basins: A case study from the Ebro Basin, N Spain. Tectonophysics 492, 150–163. https://doi.org/10.1016/j.tecto.2010.06.016

Ramsay, J.G., 1980. Shear zone geometry: A review. Journal of Structural Geology 2, 83–99. https://doi.org/10.1016/0191-8141(80)90038-3

Ramsay, J.G., Graham, R.H., 1970. Strain variation in shear belts. Can. J. Earth Sci. 7, 786–813. https://doi.org/10.1139/e70-078

Ramsay, J.G., Huber, M.I., 1987. The Techniques of Modern Structural Geology, in: Folds and Fractures, Vol. II. Academic Press, London.

Riedel, W., 1929. Zur Mechanik geologischer Brucherscheinungen. Ein Beitrag zum Problem der Fiederspatten. Zentbl. Miner. Geol. Palaont. Abt. 354–368.

Robustelli Test, C., Festa, A., Zanella, E., Codegone, G., Scaramuzzo, E., 2019. Distinguishing the Mélange-Forming Processes in Subduction-Accretion Complexes: Constraints from the Anisotropy of Magnetic Susceptibility (AMS). Geosciences 9, 381. https://doi.org/10.3390/geosciences9090381

Röller, K., Trepmann, C.A., 2008. Stereo32 v1.0.1 Software and helpfile. Ruhr-Universität Bochum, Institut für Geologie, Mineralogie & Geophysik.

Scisciani, V., 2009. Styles of positive inversion tectonics in the Central Apennines and in the Adriatic foreland: Implications for the evolution of the Apennine chain (Italy). Journal of Structural Geology 31, 1276–1294. https://doi.org/10.1016/j.jsg.2009.02.004

Sidman, D., Ferré, E.C., Teyssier, C., Jackson, M., 2005. Magnetic fabric and microstructure of a mylonite: example from the Bitterroot shear zone, western Montana. Geological Society, London, Special Publications 245, 143–163. https://doi.org/10.1144/GSL.SP.2005.245.01.07

Tarling, D., Hrouda, F., 1993. Magnetic Anisotropy of Rocks. Chapman & Hall, London.

Tavarnelli, E., 1997. Structural evolution of a foreland fold-and-thrust belt: the Umbria-Marche Apennines, Italy. Journal of Structural Geology, Fault-Related Folding 19, 523–534. https://doi.org/10.1016/S0191-8141(96)00093-4

Tavarnelli, E., 1999. Normal faults in thrust sheets: pre-orogenic extension, post-orogenic extension, or both? Journal of Structural Geology 21, 1011–1018. https://doi.org/10.1016/S0191-8141(99)00034-6

Tavarnelli, E., Butler, R.W.H., Decandia, F.A., Calamita, F., Grasso, M., Alvarez, W., Renda, P., 2004. Implications of fault reactivation and structural inheritance in the Cenozoic tectonic evolution of Italy, in: Crescenti, U., D'offizi, S., Merlino, S., Sacchi, S. (Eds.) The Geology of Italy, Società Geologica Italiana, Special Volume, 209–222.

Turtù, A., Satolli, S., Maniscalco, R., Calamita, F., Speranza, F., 2013. Understanding progressive-arc- and strike-slip-related rotations in curve-shaped orogenic belts: The case of the Olevano-Antrodoco-Sibillini thrust (Northern Apennines, Italy). J. Geophys. Res. Solid Earth 118, 459–473. https://doi.org/10.1002/jgrb.50096

Weil, A.B., Yonkee, A., 2009. Anisotropy of magnetic susceptibility in weakly deformed red beds from the Wyoming salient, Sevier thrust belt: Relations to layer-parallel shortening and orogenic curvature. Lithosphere 1, 235–256. https://doi.org/10.1130/L42.1

Xypolias, P., 2010. Vorticity analysis in shear zones: A review of methods and applications. Journal of Structural Geology 32, 2072–2092. https://doi.org/10.1016/j.jsg.2010.08.009

Table 1
Click here to download Table: Table 1.xlsx

Table 1: Summary of the anisotropy of magnetic susceptibility data at site level.

Locality	Site	Stage	n/N	χ_m (± σ) (x 10^{-9} m^3kg^{-1})	P'	T	k_1 D	k_1 I	k_1 95% conf. angles		k_3 D	k_3 I	k_3 95% conf. angles	
Sassotetto	SSR1		16/20	11.16 ± 5.19	1.040	0.785	295	32	52.1	18.3	47	31	21.1	11.6
	SSR1-SF1	E	10/16	12.71 ± 5.76	1.030	0.671	191	50	56.7	22.9	40	36	26.8	12.9
	SSR1-SF2	C	6/16	8.56 ± 2.86	1.061	0.386	304	29	18.6	8.8	51	28	13.3	8.6
Monastero	MSC1		19/20	39.65 ± 21.54	1.021	0.613	342	5	35.1	13.5	76	39	18.6	12.1
	MSC1-SF1	C	8/19	17.20 ± 4.45	1.021	0.903	161	2.3	77.5	12.0	70	32	14.4	8.9
	MSC1-SF2	C	11/19	55.98 ± 11.19	1.023	0.465	346	6	19.2	13.2	82	45	20.2	10.7
	MSC2		19/19	24.69 ± 2.66	1.017	0.648	133	13	59.4	13.0	1	71	22.2	13.8
	MSC2-SF1	A	10/19	24.12 ± 1.91	1.019	0.158	100	1	31.8	12.9	8	77	17.0	11.4
	MSC2-SF2	B	9/19	25.32 ± 3.39	1.020	0.052	169	22	28.5	14.2	351	68	32.5	14.2
Infernaccio	ISC1		19/21	22.07 ± 7.02	1.032	0.856	212	50	75.1	24.4	76	32	30.1	24.6
	ISC1-SF1	D	14/19	18.63 ± 2.86	1.014	0.479	183	35	53.3	21.6	68	31	33.8	14.9
	ISC1-SF2	E	5/19	31.71 ± 6.10	1.117	0.657	297	59	17.9	7.7	79	25	18.7	7.6
Monte Boragine	BSR2	F*	10/15	-2.03 ± 0.98	1.076	-0.351	319	59	68.7	18.1	180	25	31.9	16.0
	BSR1	F*	10/19	-3.33 ± 1.81	1.027	-0.656	169	80	70.0	31.0	9	10	43.3	23.9
	BMC1	E//	8/12	2.52 ± 1.94	1.055	0.147	250	46	59.9	27.9	4	21	52.9	20.8
	BMC2		13/16	9.83 ± 6.33	1.032	0.593	243	13	43.6	17.3	128	61	25.7	17.3
	BMC2-SF1	E or E//	6/13	6.44 ± 2.28	1.027	0.175	35	6	37.0	23.4	134	57	31.3	14.7
	BMC2-SF2	D//	7/13	12.74 ± 7.37	1.040	0.410	266	23	30.8	18.2	121	63	22.4	14.2
	BMC3		15/21	1.05 ± 2.96	1.121	-0.037	201	21	44.2	24.5	9	69	59.4	23.6
	BMC3-SF1	E or E//	8/15	3.34 ± 1.96	1.035	-0.225	211	1	49.7	20.5	304	72	45.3	28.5
	BMC3-SF2	D*	7/15	-1.56 ± 1.00	1.080	0.071	197	29	34.2	19.9	29	61	54.6	15.2
Valle Scura	VSR2		19/21	7.23 ± 1.88	1.022	0.010	207	25	32.2	17.8	31	65	35.3	16.6
	VSR2-SF1	E//	14/19	7.12 ± 1.80	1.027	-0.383	211	25	23.3	16.7	28	65	43.5	15.2
	VSR2-SF2	F	5/19	7.52 ± 2.29	1.020	-0.134	132	4	23.0	12.1	35	59	22.7	15.6
	VSR1	E//	23/24	9.29 ± 2.17	1.039	0.091	230	28	24.3	18.0	67	61	24.3	18.0
	VMC1		18/21	8.56 ± 3.56	1.015	0.529	263	21	68.5	14.8	29	57	33.5	18.7
	VMC1-SF1	E//	10/18	8.16 ± 2.22	1.020	-0.346	227	26	22.5	18.6	1	55	45.1	21.6
	VMC1-SF2	F	8/18	9.07 ± 4.89	1.023	-0.361	303	5	28.3	9.6	38	42	46.0	10.3
	VCM2		19/21	12.25 ± 2.37	1.024	0.406	234	21	49.0	15.8	37	68	22.7	15.8
	VMC2-SF1	D//	9/19	12.25 ± 2.37	1.032	-0.004	253	19	11.6	10.5	43	68	28.2	8.7
	VMC2-SF2	E	10/19	12.42 ± 1.51	1.020	0.186	191	20	25.6	14.1	28	69	26.8	14.9
	VCM3		18/21	11.56 ± 3.62	1.022	0.442	204	22	44.0	20.6	60	64	28.3	20.1
	VMC3-SF1	D//	8/18	11.44 ± 3.24	1.025	0.120	244	38	30.4	17.3	64	53	23.6	21.8
	VMC3-SF2	E	10/18	12.18 ± 4.37	1.025	0.181	185	12	21.0	15.1	37	77	25.9	16.3
Cottanello	CSR1		13/15	2.97 ± 1.21	1.025	-0.056	317	35	50.4	26.9	204	29	39.4	26.3
	CSR1-SF1	D	6/13	2.4 ± 1.37	1.039	0.113	325	42	53.5	22.8	188	39	36.8	21.3
	CSR1-SF2	C	7/13	3.47 ± 0.86	1.019	0.097	312	17	51.2	11.4	221	5	30.5	11.4
	CSR2		16/22	5.72 ± 2.79	1.026	0.058	329	22	47.5	25.1	167	67	47.6	23.0
	CSR2-SF1	E	8/16	5.91 ± 2.78	1.045	0.222	13	40	22.2	13.5	188	50	14.6	13.0
	CSR2-SF2	C	8/16	5.52 ± 2.97	1.038	0.329	324	4	32.8	12.9	60	57	27.4	13.6
	CSR3		15/20	6.76 ± 4.20	1.042	0.453	12	18	56.0	26.6	228	68	26.8	10.8
	CSR3-SF1	E	9/15	5.80 ± 4.30	1.049	-0.026	20	16	36.0	26.5	240	69	26.8	14.6
	CSR3-SF2	C	6/15	8.19 ± 3.97	1.042	0.395	308	1	37.4	8.0	217	61	20.9	4.8

Columns: Locality; Site; Stage = degree of deformation from sedimentary fabric (A) to latest tectonic event (F), (*)inverse fabric and (//)tectonic fabric parallel to the transport direction; n/N = number of specimens accepted/number of specimens measured; χm = mean mass magnetic susceptibility (10-9m3kg-1) and

Figure 1

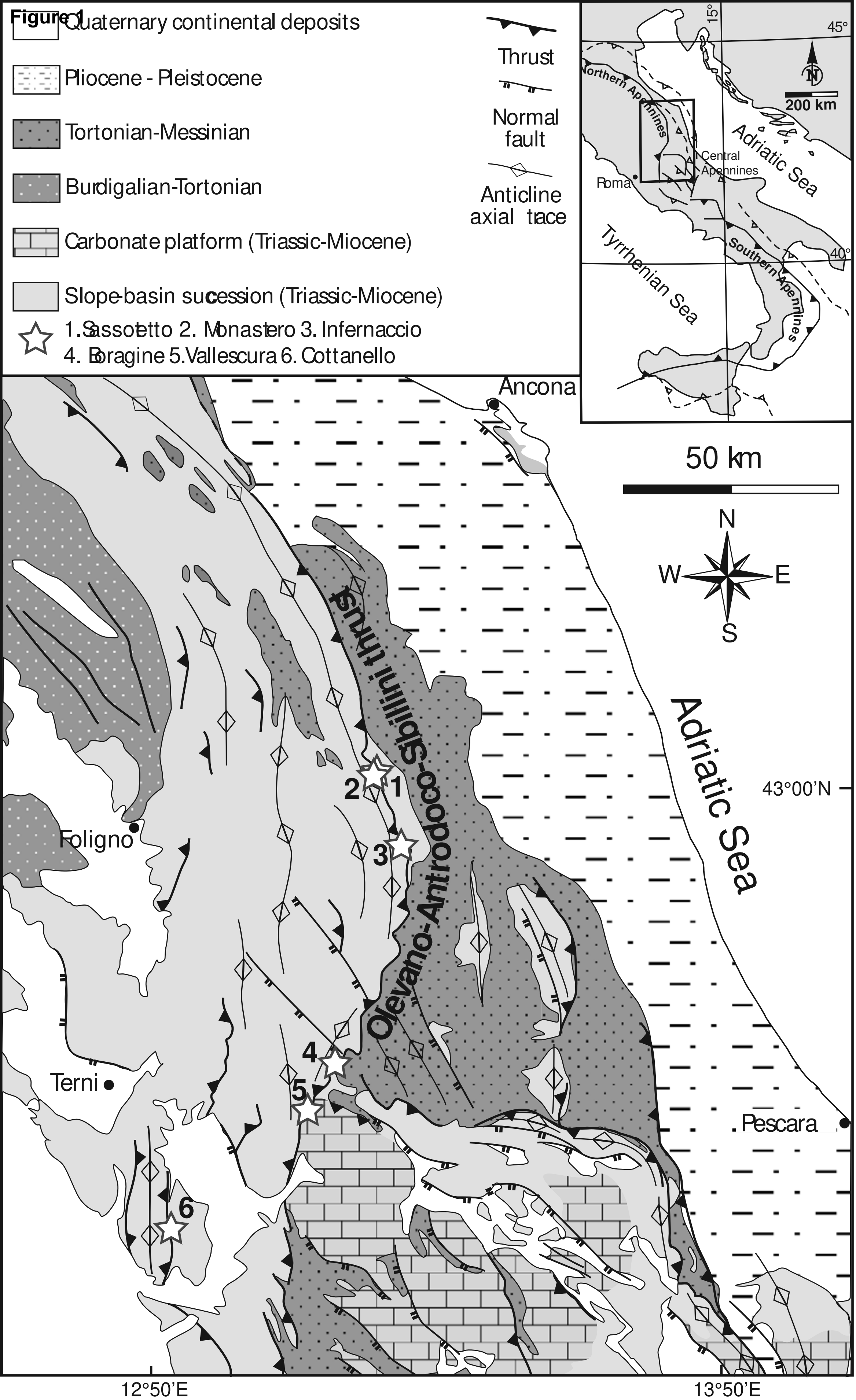

Figure 1: Schematic geological map of the Northern Apennines (Italy) with the studied localities (white stars), modified after Calamita et al. (2012). The curve-shaped Olevano-Antrodoco-Sibillini (OAS) thrust is the outer front of the Northern Apennines.

Figure 2

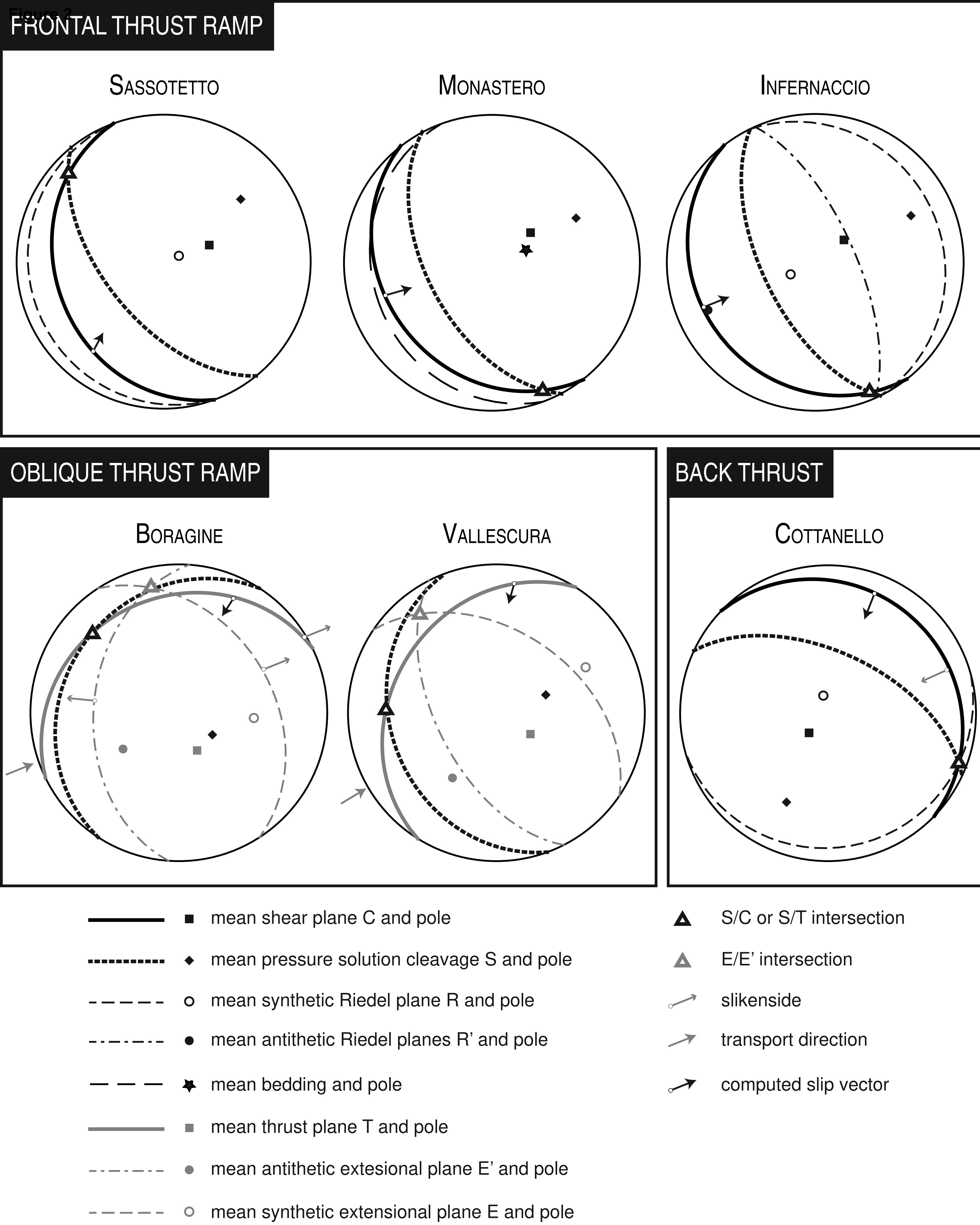

Figure 2: Summary of the structural data for each studied locality integrated with data from the literature (Calamita et al., 2012; Turtù et al., 2013; Pace et al., 2015).

Figure 3

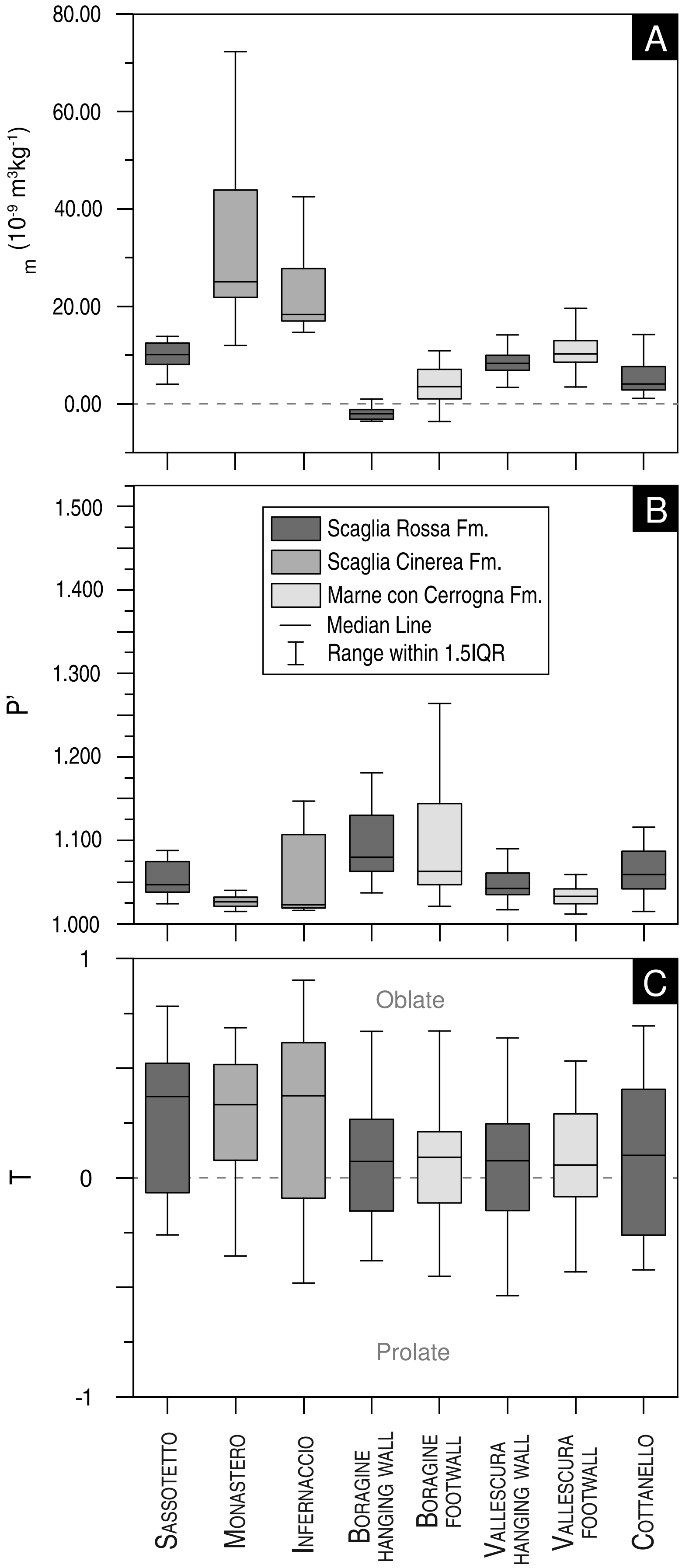

Figure 3: Box-and-whisker plots of the a) mass magnetic susceptibility (m), b) corrected anisotropy degree (P') and c) shape parameter (T) for the studied localities. Central boxes include values between the lower and upper quartiles. Di erent gray shades correspond to di erent lithologies.

Figure 4

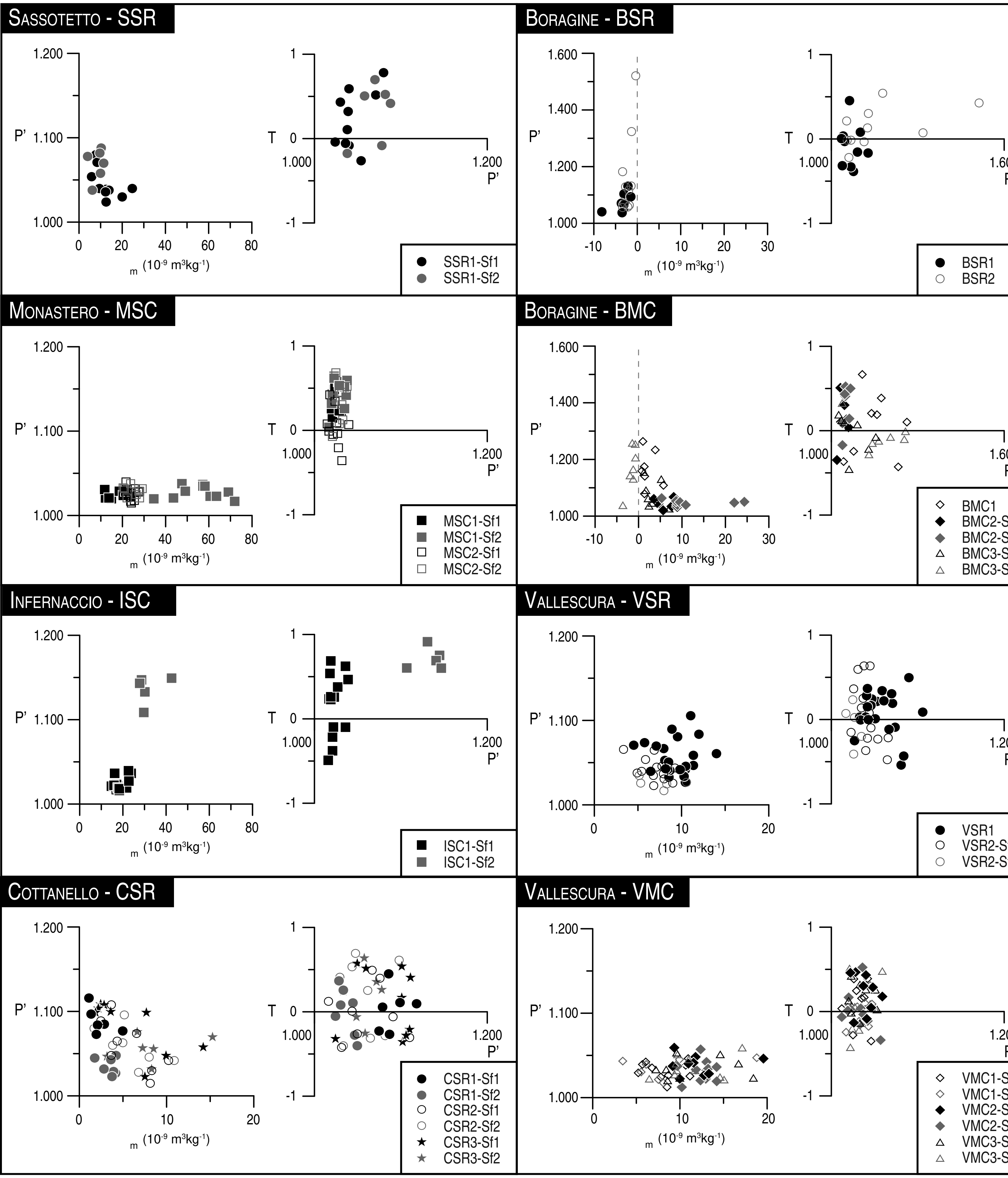

Figure 4: Corrected anisotropy degree (P’) vs. mass susceptibility (m) and shape parameter (T) vs. correct anisotropy degree (P’) plots for the various localities. Different symbols correspond to different lithologie circles and stars for Scaglia Rossa Fm., squares for Scaglia Cinerea Fm. and lozenges and triangles for Mar con Cerrogna Fm.

Figure 5

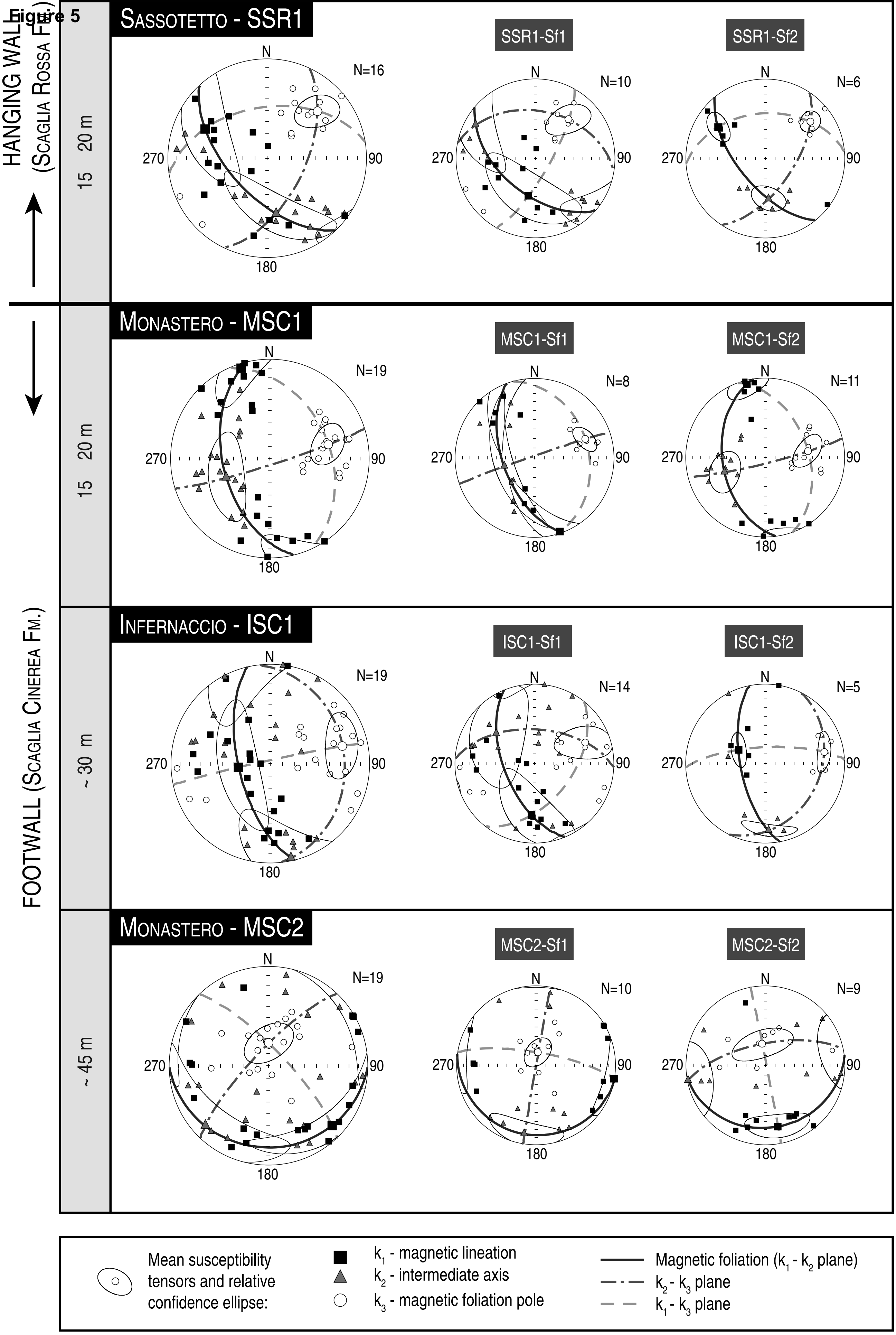

Figure 5: Magnetic fabric from the frontal thrust ramp at Sassotetto, Monastero (sites MSC1 and MSC2) and Infernaccio. Equal area projections in geographic coordinates of the principal magnetic susceptibility axes at site level (left) and relative subfabrics (middle and right).

Figure 6

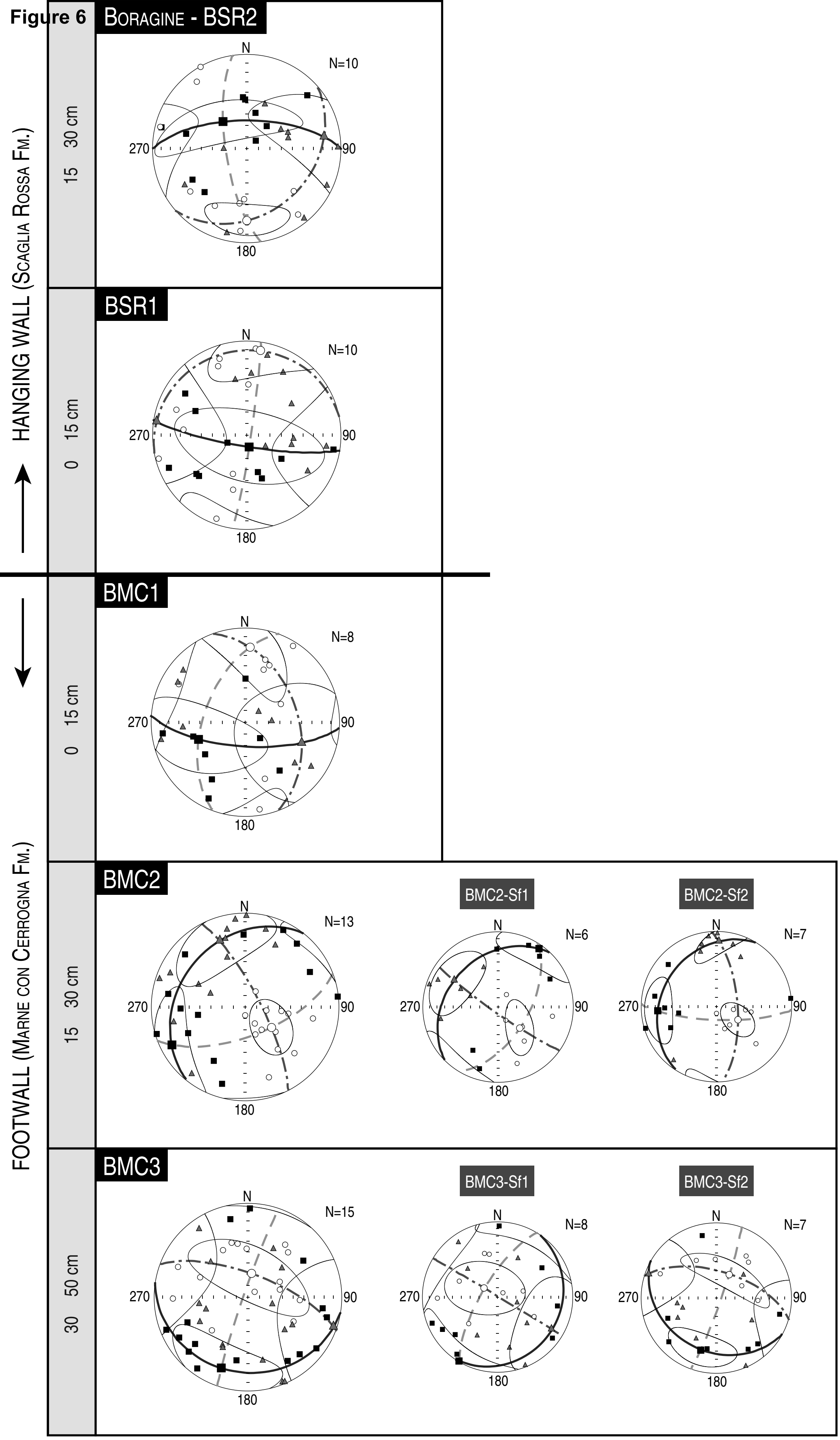

Figure 6: Magnetic fabric from the oblique thrust ramp at Boragine. Equal area projections in geographic coordinates of the principal magnetic susceptibility axes at site level (left) and relative subfabrics when detected (middle and right). Legend as in Figure 5.

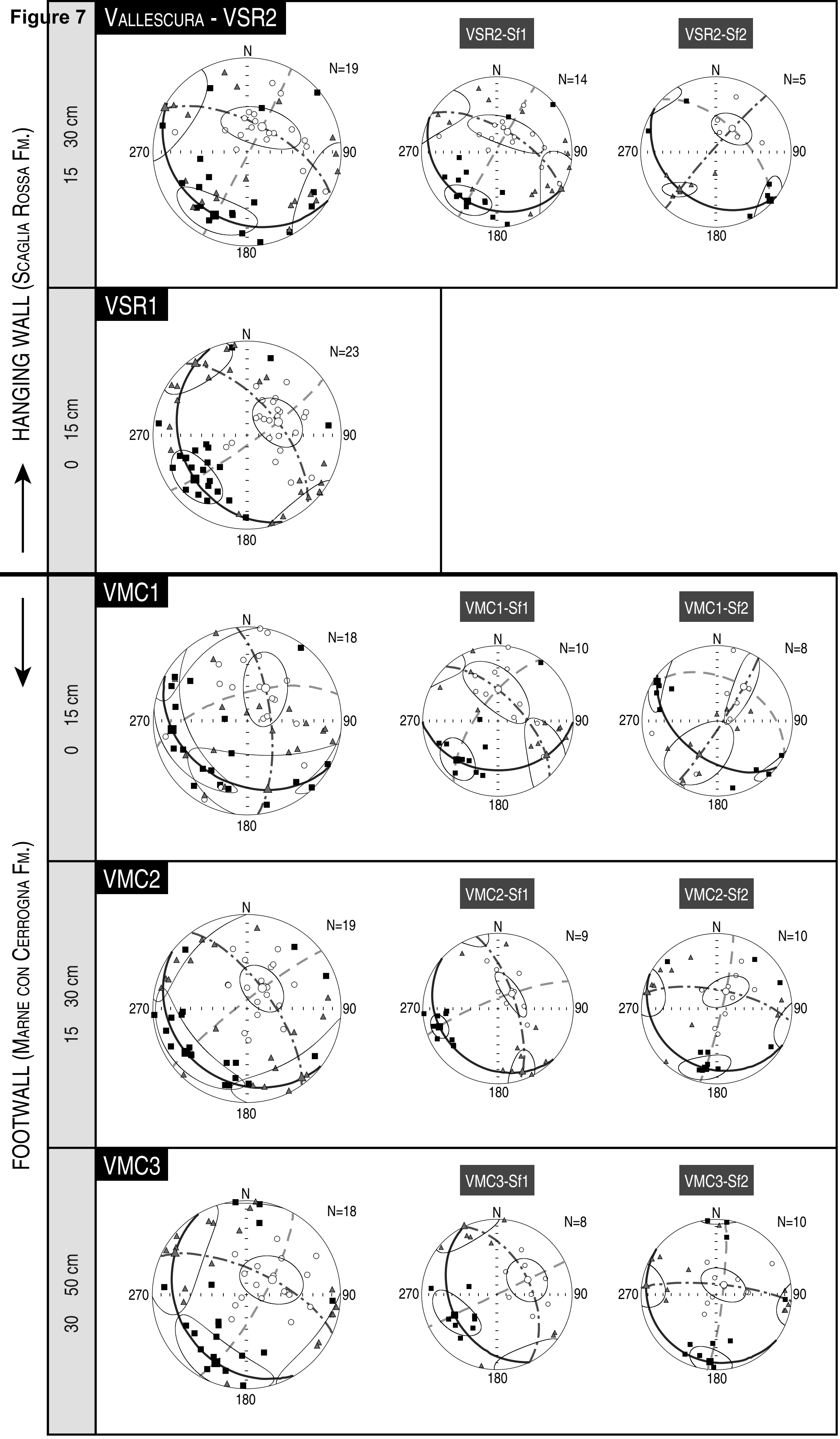

Figure 7: Magnetic fabric from the oblique thrust ramp at Vallescura. Equal area projections in geographic coordinates of the principal magnetic susceptibility axes at site level (left) and relative subfabrics when detected (middle and right). Legend as in Figure 5.

Figure 8

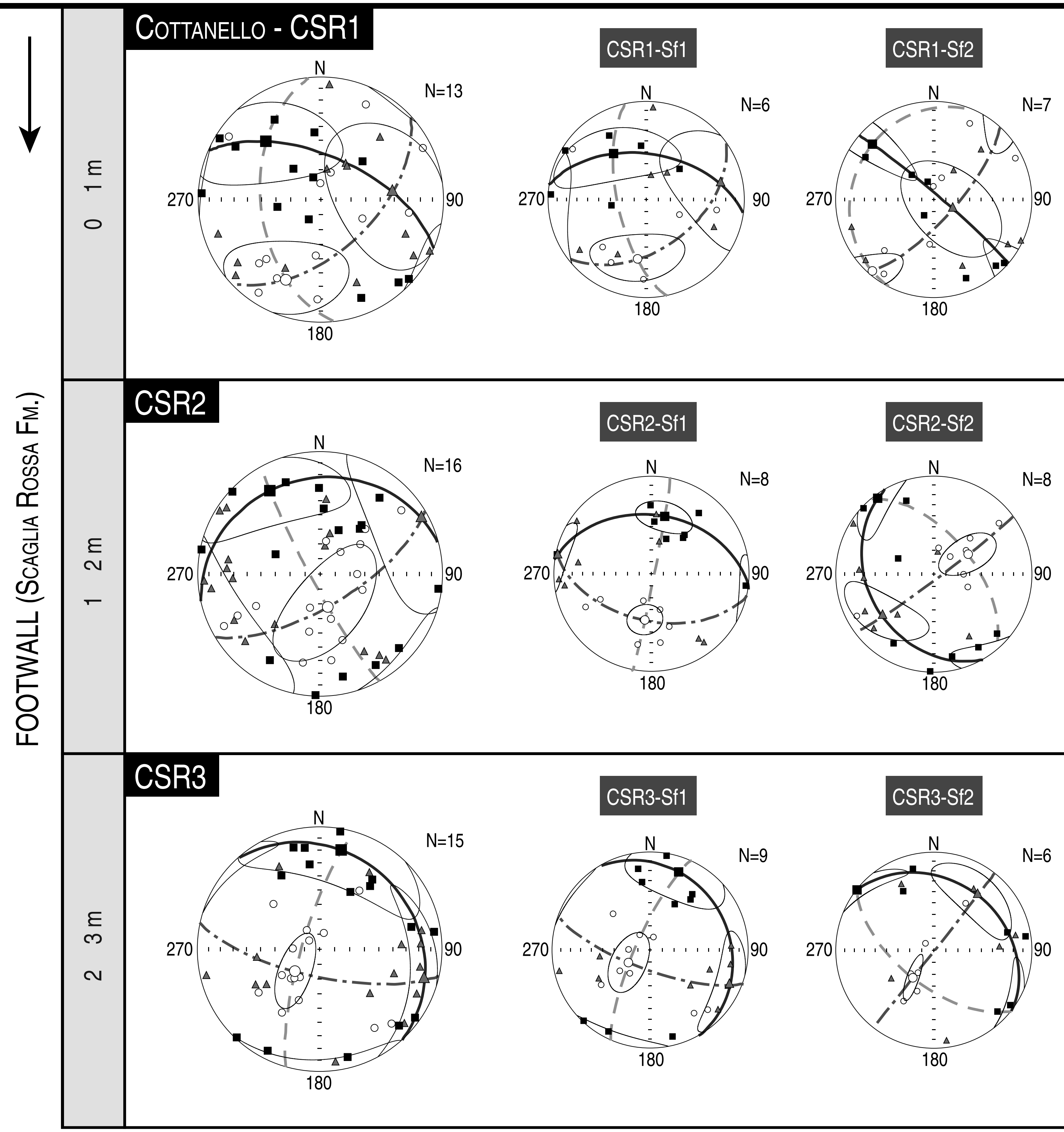

Figure 8: Magnetic fabric from the back-thrust at Cottanello. Equal area projections in geographic coordinates of the principal magnetic susceptibility axes at site level (left) and relative subfabrics (middle and right). Legend as in Figure 5.

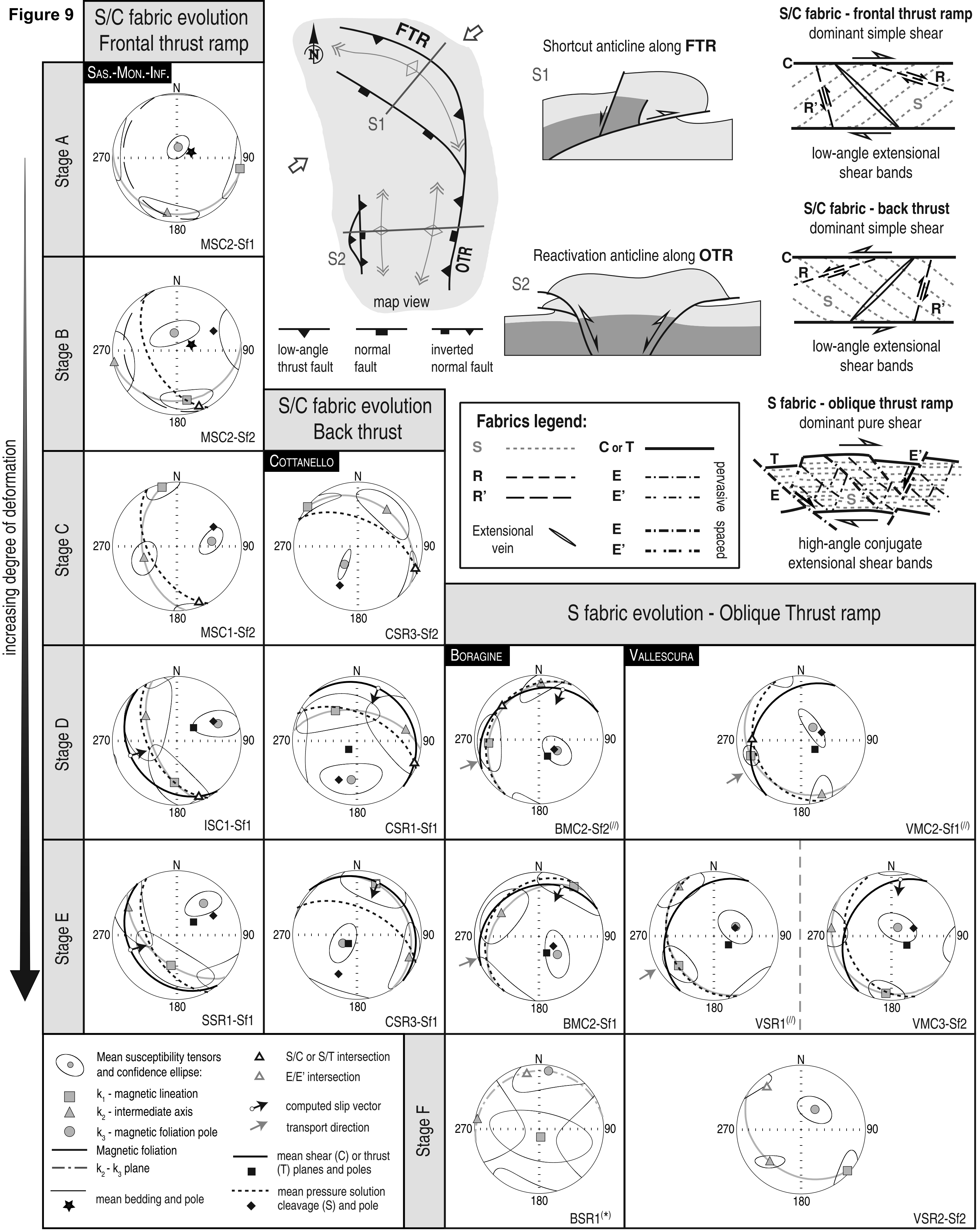

Figure 9: Summary of magnetic fabric stages and comparison with structural data. Representative examples from the different deformation regimes are reported. Conceptual diagram of the different types of shear deformation fabric (ZX section of strain ellipses) related to frontal (FTR) and oblique (OTR) thrust ramps (modified from Calamita et al., 2012; Pace et al., 2015).

Supplementary material - Table 2
Click here to download Supplementary material for online publication only: SupTable2_.xlsx

*Declaration of Interest Statement

Declaration of interests

☒ The authors declare that they have no known competing financial interests or personal relationships that could have appeared to influence the work reported in this paper.

☐The authors declare the following financial interests/personal relationships which may be considered as potential competing interests:

Author contributions

SS: Project administration, funding acquisition, conceptualization, field work, methodology, laboratory analysis, structural analysis, writing - original draft.

CRT: field work, laboratory analysis, data curation, structural analysis, methodology, formal analysis, writing - original draft, data visualization

DS: field work, laboratory analysis, writing - review and editing

EZ: supervision, funding acquisition, field work, writing - original draft, data visualization

FC: field work, structural analysis, writing - review and editing

ET: field work, laboratory analysis, writing - review and editing